

1 **Assessing the influence of water sampling strategy on the performance of tracer-**
2 **aided hydrological modeling in a mountainous basin on the Tibetan Plateau**

3 Yi Nan¹, Zhihua He², Fuqiang Tian¹, Zhongwang Wei³, Lide Tian⁴

4 ¹ Department of Hydraulic Engineering, State Key Laboratory of Hydrosience and Engineering,
5 Tsinghua University, Beijing, China

6 ² Center for Hydrology, University of Saskatchewan, Saskatchewan, Canada

7 ³ Guangdong Province Key Laboratory for Climate Change and Natural Disaster Studies, School of
8 Atmospheric Sciences, Sun Yat-sen University, Guangzhou, Guangdong, China

9 ⁴ Institute of International Rivers and Eco-security, Yunnan University, Kunming, China

10 ***Corresponding to:*** Fuqiang Tian

11 Email: tianfq@tsinghua.edu.cn

12

13 **Abstract**

14 Tracer-aided hydrological models integrating water isotope module into the simulation of
15 runoff generation are useful tools to reduce uncertainty of hydrological modeling in cold basins
16 that are featured by complex runoff processes and multiple runoff components. However, there
17 is little guidance on the strategy of field water sampling for isotope analysis to run tracer-aided
18 hydrological models, which is especially important for large mountainous basins on the Tibetan
19 Plateau (TP) where field water sampling work is highly costly. This study conducted a set of
20 numerical experiments based on the THREW-T (Tsinghua Representative Elementary
21 Watershed - Tracer-aided version) model to evaluate the reliance of the tracer-aided modeling
22 performance on the availability of site measurements of water isotope in the Yarlung Tsangpo
23 River (YTR) basin on the TP. Data conditions considered in the numerical experiments included
24 the availability of glacier meltwater isotope measurement, quantity of site measurements of
25 precipitation isotope, and the variable collecting strategies for stream water sample. Our results
26 suggested that: (1) In high-mountain basins where glacier meltwater samples for isotope
27 analysis are not available, estimating glacier meltwater isotope by an offset parameter from the
28 precipitation isotope is a feasible way to force the tracer-aided hydrological model. Using a set
29 of glacier meltwater $\delta^{18}\text{O}$ that were 2‰~9‰ lower than the mean precipitation $\delta^{18}\text{O}$ resulted in
30 only small changes in the model performance and the quantifications of contributions of runoff
31 components (CRCs, smaller than 5%) to streamflow in the YTR basin; (2) strategy of field
32 sampling for site precipitation to correct the global gridded isotope product of isoGSM for
33 model forcing should be carefully designed. Collecting precipitation samples at sites falling in
34 the same altitude tends to be worse at representing the ground pattern of precipitation $\delta^{18}\text{O}$ over
35 the basin than collecting precipitation samples from sites in a range of altitudes; (3) Collecting
36 weekly stream water samples at multiple sites in the wet and warm seasons is the optimal
37 strategy for calibrating and evaluating a tracer-aided hydrological model in the YTR basin. It is
38 highly recommended to increase the number of stream water sampling sites rather than
39 spending resource on extensive sampling of stream water at a sole site for multiple years. These
40 results provide important implications for collecting site measurements of water isotope for
41 running tracer-aided hydrological models to improve quantifications of CRCs in the high-
42 mountain basins.

43

44 **1. Introduction**

45 Catchments located in mountainous regions generally provide important water resources
46 for downstream regions (Viviroli et al., 2003). As typical mountainous cryosphere, the Tibetan
47 Plateau (TP) is the source region for several large rivers in Asia, and has been called as a ‘water
48 tower’ because of its importance for downstream livelihoods and agricultural irrigations
49 (Schaner et al., 2012). Dominant characteristic of mountainous catchments on TP is the
50 multiphase of water sources that generate runoff and the consequently complex hydrological
51 processes, highlighting the importance of accurately quantifying the contributions of runoff
52 components (CRCs) to streamflow for better understandings the runoff dynamics under
53 changing climate. This task is difficult due to the complex hydrological processes being
54 insufficiently represented by typical hydrological models, leading to large uncertainty of
55 hydrological simulations (He et al., 2018). Due to the strong inter-compensation of runoff
56 processes induced by different water sources and runoff pathways (Duethmann et al., 2015),
57 uncertainties of the modeled CRCs in mountainous basins on the TP are rather high. Utilizing
58 more datasets to evaluate the model performance is a feasible way to constrain modeling
59 uncertainty and improve quantifications of CRCs in cold regions (Chen et al., 2017).

60 Tracer-aided hydrological models integrating environmental tracer (e.g., stable oxygen
61 isotope, ^{18}O) modules into runoff generation processes have proved helpful for parameter
62 calibration, model structure diagnosis and CRC quantification (Son and Sivapalan, 2007; Birkel
63 et al., 2011), and are increasingly adopted in cold catchments (e.g., Ala-aho et al., 2017; He et
64 al., 2019; Nan et al., 2021a). Recent studies indicated that estimates of precipitation $\delta^{18}\text{O}$ from
65 outputs of isotopic general circulation models (iGCMs) perform well on forcing tracer-aided
66 models in large basins with a high cost of water sampling (Delavau et al., 2017; Nan et al.
67 2021b). Similarly to the tracer-based end-member mixing methods that utilize the different
68 tracer signatures of water sources to separate the hydrograph and quantify CRCs (Klaus and
69 McDonnell, 2013; He et al., 2020), the tracer-aided hydrological models used the differed
70 isotopic compositions of runoff components to regulate the water apportionments in runoff
71 generation. The isotopic compositions of runoff components strongly differ in high-mountain
72 basins resulting from the following two reasons: One is the significantly more depleted $\delta^{18}\text{O}$ of
73 meltwater compared to that of rain, due to the altitude and temperature effects, and the
74 fractionation effect during melting processes (Xi, 2014; Boral and Sen, 2020). Another is the
75 damping and lagging isotopic variability of subsurface runoff pathway, compared to that of
76 surface runoff, as a result of the catchment hydrological functions of storing, mixing and
77 transporting water (Bowen et al., 2019; Birkel and Soulsby, 2015; McGuire and McDonnell,
78 2006). Consequently, water isotope signatures show potential to improve the representations of
79 internal hydrological processes in hydrological models, if observations of water isotopes were
80 involved in the model calibration and evaluation procedures (McGuire et al., 2007; He et al.,

81 2019).

82 Although a plenty of isotope-based works have been conducted in mountainous
83 catchments on the TP to improve understandings of local hydrological processes (e.g., Li et al.,
84 2020; Kong et al., 2019; Tan et al., 2021), few of them provided guidance on data collection of
85 water isotope for hydrological applications in large mountainous areas. Some water sampling
86 works in large mountainous catchments were conducted in a single field campaign (e.g., Xia et
87 al., 2019; Dong et al., 2018), which is, although helpful to understand the generations of short-
88 term runoff events, not suitable for the calibration of tracer-aided models in a multi-year
89 simulation period (Knapp et al., 2019; Zhang et al., 2019). An exception is Stevenson et al.
90 (2021) who utilized a 7-year dataset of stream water $\delta^{18}\text{O}$ in a 3.2 km² catchment to analyze the
91 effects of stream water sampling strategies on the calibration of a tracer-aided hydrological
92 model. Challenges arise when transferring their findings to the application of tracer-aided
93 hydrological models in large high-mountain basins: First, it is questionable that whether
94 sampling stream water at one site can adequately represent the isotope signature of stream water
95 over the whole large basin, considering the strong spatial variability of hydrological processes
96 caused by the heterogeneity in meteorological factors and land surface conditions in mountains
97 (Wang et al., 2021; Li et al., 2020). Second, the influences of data collection of precipitation
98 isotope on the performance of tracer-aided hydrological models remain unclear. Results of He
99 et al. (2019) indicated that monthly sampling of precipitation at two sites seems to be able to
100 capture the isotope variations in a 233 km² catchment. However, the requirement of isotope
101 data quantity to adequately capture the spatial pattern of precipitation isotope signature for
102 forcing tracer-aided models in large basins ($\sim 10^5$ km²) is poorly explored (Nan et al., 2021b).
103 Third, in glacierized mountainous catchments where streamflow was fed by additional water
104 source of glacier melt, the requirement of glacier meltwater samples for the forcing and
105 evaluation of tracer-aided hydrological models is also unclear. Consequently, better
106 understandings of how water sampling strategies influence the value of water isotope data for
107 aiding hydrological modeling, is highly helpful for guiding the establishment of monitoring
108 systems of water isotope in large mountainous regions. Considering the high costs of human
109 and financial resources of collecting water samples in TP area, it is important to take efficient
110 strategies for water sampling that balance the trade-off between field work burden and data
111 adequacy well (Sprenger et al., 2019).

112 Motivated by the mentioned backgrounds, we conducted detailed analysis on the tracer-
113 aided model performance in a large mountainous basin on the TP under different assumed
114 situations with respect to the collection strategy of site water isotope data, based on a numerical
115 experiment method. We adopted the tracer-aided hydrological model THREW-T developed by
116 Nan et al. (2021a), which was forced by the global gridded isotope outputs of iGCM being
117 merged with measurements of precipitation $\delta^{18}\text{O}$, to achieve the research aim. Three specific

118 questions were addressed: (1) how does the estimated isotopic composition of glacier meltwater
119 influence the performance of tracer-aided hydrological modeling when no glacier meltwater
120 samples were available, (2) how does the collection strategy of site precipitation samples for
121 precipitation isotope data merging influence the model performance, and (3) how does the
122 sampling strategy of stream water influence the model calibration and evaluation? This study
123 focused on the sampling strategy of precipitation and stream water, while the influence of
124 glacier/snow meltwater isotope data sampling was not within the scope of this study.

125 **2. Materials and methodology**

126 **2.1 Study area**

127 The Yarlung Tsangpo River (YTR) basin, located in the southern TP (Fig. 1), extends in
128 the ranges of 27°N -32°N and 82°E -97°E, with an elevation extent of 2900-6900 m above sea
129 level (a.s.l.), which is one of the largest basins on the TP. The mean annual precipitation in the
130 YTR basin is around 470mm featured by a distinct wet season from June to September, due to
131 the dominance of the South Asian monsoon. Drainage area above the Nuxia hydrological station
132 at the basin outlet is approximately 2×10^5 km², and around 2% of which is covered by glacier.

133 The Karuxung River (KR) catchment is located in the upper regions of the YTR basin, and
134 was chosen as a supplementary experiment catchment, because of the long term field work of
135 water sampling in this catchment. The KR originates from the Lejin Jangsan peak of the Karola
136 mountain (7206m a.s.l.), and flows into the Yamdrok Lake (4550m a.s.l.), draining an area of
137 around 286 km². Streamflow in the KR catchment is strongly influenced by glaciers which
138 cover an area of 58 km².

139 **[Figure 1]**

140 **2.2 Hydro-meteorological and water isotope data**

141 Elevation of the YTR basin was derived from a digital elevation model (DEM) with a
142 spatial resolution of 30m from the Geospatial Data Cloud (<https://www.gscloud.cn>). Daily
143 meteorological inputs including precipitation, temperature and potential evapotranspiration
144 were collected from the 0.1°×0.1° China Meteorological Forcing Dataset (CMFD, Yang and
145 He, 2019). The second glacier inventory data set of China (Liu, 2012) and the Tibetan Plateau
146 Snow Cover Extent product (TPSCE, Chen et al., 2018) were used to denote the glacier and
147 snow coverages. Vegetation coverages were extracted from the MODIS satellite products of
148 eight-day leaf area index (LAI) dataset MOD15A2H (Myneni et al., 2015) and monthly
149 normalized difference vegetation index (NDVI) dataset MOD13A3 (Didan et al., 2015). Soil
150 types and properties in the tested basins were collected from the Harmonized World Soil
151 Database (HWSD, He, 2019). Observations of daily streamflow during 2000-2015 at the Nuxia,

152 and that during 2000-2010 at Yangcun and Nugesha stations were used for hydrological model
 153 evaluation.

154 In the KR catchment, daily temperature and precipitation during 2006-2012 were collected
 155 at the Langkazi meteorological station. Altitudinal distributions of temperature and
 156 precipitation across the KR catchment were estimated based on the lapse rates reported in
 157 Zhang et al. (2015). Daily streamflow during 2006-2012 was measured at the Wengguo
 158 hydrological station.

159 Outputs of the scripps global spectral model with water isotopes incorporated (isoGSM,
 160 Yoshimura et al., 2008) with the spatial and temporal resolutions of $1.875^\circ \times 1.875^\circ$ and 6h were
 161 extracted to represent the spatio-temporal pattern of the precipitation isotope in the YTR basin.
 162 According to a previous evaluation of the isoGSM product (Nan et al., 2021b), while it can
 163 effectively capture the seasonal variation of precipitation $\delta^{18}\text{O}$, it had two major flaws: it
 164 overestimated precipitation $\delta^{18}\text{O}$ in the YTR basin, and performed poorly on accurately
 165 capturing the isotope signature of specific precipitation events and time periods. Higher
 166 elevation stations typically had a stronger bias. To obtain measurement precipitation $\delta^{18}\text{O}$ data,
 167 grab samples of precipitation were collected in the wet season of 2005 at four stations along the
 168 main channel of YTR, i.e., Nuxia (3691 m a.s.l.), Yangcun (4541m a.s.l.), Nugesha (4715m
 169 a.s.l.) and Lazi (4889m a.s.l.). The precipitation water samples were collected as soon as
 170 possible after the precipitation event in order to avoid the effect of evaporation. Stream water
 171 samples were collected weekly during the same period from river at the four stations.

172 The isoGSM isotope products were merged with measurement precipitation isotope data
 173 according to Eqs. 1-3 to provide input data for model: First, the bias of isoGSM product was
 174 assumed to be linearly related to altitude. Relation between the mean bias of isoGSM products
 175 and altitude was estimated by a least square method using $\delta^{18}\text{O}$ measurements of precipitation
 176 samples and gridded isoGSM estimates at the four sampling sites (Eqs. 1-2); Second, in each
 177 REW, precipitation $\delta^{18}\text{O}$ was determined by Eq. 3, based on the average altitude and the
 178 availability of $\delta^{18}\text{O}$ measurements from precipitation site samples on the date.

$$179 \quad B_i = \overline{\delta^{18}O_{i,M}} - \overline{\delta^{18}O_{i,G}} \quad (1)$$

$$180 \quad B = a \cdot H + b \quad (2)$$

$$181 \quad \delta^{18}O_{k,j,\text{Merged}} = \begin{cases} \delta^{18}O_{k,j,G} + B_k, & \text{for date } j \text{ with no data} \\ \frac{\sum_{i=1}^4 \delta^{18}O_{i,j,M}}{4} - \frac{\sum_{i=1}^4 \overline{\delta^{18}O_{i,M}}}{4} + \overline{\delta^{18}O_{k,G}} + B_k, & \text{for date } j \text{ with data, but unit } k \text{ containing no sampling site} \\ \delta^{18}O_{k,j,M}, & \text{for date } j \text{ with data, and unit } k \text{ containing sampling site} \end{cases} \quad (3)$$

182 where, B_i is the bias of isoGSM at sites i . $\overline{\delta^{18}O_{i,M}}$ and $\overline{\delta^{18}O_{i,G}}$ are the weighted average of the
 183 site measurement and isoGSM estimate over the sampling period at sites i , respectively. H is
 184 the altitude of the sampling site. Parameters a and b are the linear regression coefficients, which
 185 were estimated as -0.0046 and 14.96 by the least square method in this study. $\delta^{18}O_{k,j,\text{Merged}}$

186 is the precipitation isotope obtained by merging isoGSM and measurement data, and $\delta^{18}O_{k,j,G}$
187 refers to the original isoGSM isotope estimate at the hydrological model unit k on the date j .

188 Glacier meltwater $\delta^{18}O$ was assumed to be constantly lower than the weighted average of
189 precipitation $\delta^{18}O$ by an offset parameter ($\Delta\delta$) during the study period (Eq. 4) because of the
190 unavailability of glacier meltwater samples, which is generally within the range of 2-9‰ in the
191 worldwide mountain regions (Rai et al., 2019; Wang et al., 2016; He et al., 2019; Ohlanders et
192 al., 2013; Jeelani et al., 2017) and is adopted as 5‰ from Boral and Sen (2020) in the YTR
193 basin.

$$194 \quad \delta^{18}O_{k,GM} = \overline{\delta^{18}O_{k,Corr}} - \Delta\delta \quad (4)$$

195 In the KR catchment, grab samples of precipitation and stream water were collected at the
196 Wengguo station in 2006-2007 and 2010-2012 for isotope analysis. The spatial distribution of
197 precipitation $\delta^{18}O$ was estimated based on an altitudinal lapse of -0.34‰/100 as reported in Liu
198 et al. (2007). Glacier meltwater $\delta^{18}O$ was assumed to be constantly as -18.9‰ during the study
199 period (as reported by Gao et al. 2009). Details of precipitation and stream water samples in the
200 YTR and KR catchments were summarized in Table 1.

201 **[Table 1]**

202 **2.3 Tracer-aided hydrological model**

203 A distributed tracer-aided hydrological model, THREW-T (Tsinghua Representative
204 Elementary Watershed - Tracer-aided version) model developed by Tian et al. (2006) and Nan
205 et al. (2021a) was adopted for streamflow and isotope simulations. This model uses the
206 representative elementary watershed (REW) method for spatial discretization of catchments
207 (Reggiani et al., 1999). The study catchment is first divided into REWs based on DEM, and
208 each REW is further divided into two vertical layers (surface and subsurface layers), including
209 eight hydrological subzones based on the land cover and soil properties. In total, 63 and 41
210 REWs were extracted for the YTR basin and KR catchment, respectively (Tian et al., 2020;
211 Nan et al., 2021a, 2021b). Areal averages of the gridded estimates of meteorological variables,
212 vegetation cover and soil property were calculated in each REW to drive the model. A module
213 representing glacier melting and snowpack evolution was incorporated into the model for
214 application in cold regions (He et al., 2015; Xu et al., 2019; Tian et al., 2020). Accumulation
215 and melting processes of snowpack were simulated according to temperature and precipitation,
216 to update the snow water equivalent (SWE) of each REW. The snow cover area (SCA) was then
217 calculated using the snow cover depletion curve (Fassnacht et al., 2016) and SWE threshold
218 value (Parajka and Blöschl, 2008) for YTR basin and KR catchment, respectively, due to the
219 different catchment scales. For simplification, the evolution of glacier was not simulated in the
220 model. The temperature-index approach was used to calculate the amount of glacier melting,

221 and it was assumed that the glacier melting water would directly contribute to streamflow
222 through surface runoff pathway.

223 The tracer-aided module was developed by Nan et al. (2021a). The isotope was assumed
224 to mix completely in each hydrological simulation unit within a simulation step. The Rayleigh
225 fractionation method was adopted to simulate the isotope fractionation during water
226 evaporation (similarly to He et al. 2019, Hindshaw et al. 2011, Wolfe et al. 2007). No parameters
227 related to isotope modeling were introduced, since the isotope concentration was updated based
228 on the water content of each unit and fluxes among them, which have been calculated in the
229 runoff generation and flow concentration modules of the model. Forced by the inputs of
230 precipitation and glacier meltwater isotopic compositions, the model simulates the isotope
231 evolution in all the water storages in the watershed, including stream water, soil water and
232 snowpack. The glacier evolution processes were not simulated in the hydrological model,
233 therefore an assumed constant value was adopted to determine the isotope mass carried by
234 glacier meltwater, instead of updating the isotope composition of glacier like other water
235 storages. The iGCM isotope products properly corrected by $\delta^{18}\text{O}$ measurements of precipitation
236 samples have proved feasible to force the THREW-T model in large catchments like YTR on
237 the TP (Nan et al., 2021b). More details of hydrological model together with the snowpack
238 evolution and tracer-aided module are given in Tian et al. (2006) and Nan et al. (2021a)

239 The THREW-T model quantified the contributions of runoff components (CRC) to
240 streamflow based on two definitions of runoff components as reviewed in He et al. (2021). The
241 first definition is based on the individual water sources in the total water input triggering runoff
242 processes, including rainfall, snowmelt and glacier melt. The second definition is based on
243 pathways of runoff-generation processes, resulting in surface and subsurface runoff (baseflow).

244 Physical basis and value ranges of the calibrated parameters in the THREW-T model were
245 described in Table 2. The value of parameter was assumed to be universal for all the REWs.
246 Two kinds of calibration approaches were conducted: (1) a bi-objective calibration using
247 discharge and SCA, and (2) a tri-objective calibration using discharge, SCA and stream water
248 $\delta^{18}\text{O}$. Metrics used to evaluate the model performance are listed in Eqs. 5-8. The Nash-Sutcliffe
249 efficiency coefficient (NSE) was used to optimize the simulation of discharge and isotope,
250 whereas the root-mean-square error (RMSE) was used for the evaluation of SCA simulation.
251 The Logarithmic Nash-Sutcliffe efficiency coefficient (lnNSE) was used additionally for
252 discharge calibration to assess the simulation of baseflow. The model parameters were
253 calibrated by streamflow and SCA observations during 2001-2010 (at Nuxia station) and 2006-
254 2012 in the YTR and KR basins, respectively. The model performance in YTR basin was
255 validated by the Nuxia streamflow and SCA observations during 2011-2015, and the
256 streamflow observations at Yangcun and Nugesha stations during 2001-2010.

$$257 \quad NSE_{\text{dis}} = 1 - \frac{\sum_{i=1}^n (Q_{o,i} - Q_{s,i})^2}{\sum_{i=1}^n (Q_{o,i} - \bar{Q}_o)^2} \quad (5)$$

$$258 \quad NSE_{\text{Indis}} = 1 - \frac{\sum_{i=1}^n (\ln Q_{o,i} - \ln Q_{s,i})^2}{\sum_{i=1}^n (\ln Q_{o,i} - \ln \bar{Q}_o)^2} \quad (6)$$

$$259 \quad RMSE_{\text{SCA}} = \sqrt{\frac{\sum_{i=1}^n (SCA_{o,i} - SCA_{s,i})^2}{n}} \quad (7)$$

$$260 \quad NSE_{\text{iso}} = 1 - \frac{\sum_{i=1}^n (\delta^{18}O_{o,i} - \delta^{18}O_{s,i})^2}{\sum_{i=1}^n (\delta^{18}O_{o,i} - \bar{\delta^{18}O_o})^2} \quad (8)$$

261 where, n is the total number of observations. Subscripts of “o” and “s” refer to observed and
 262 simulated variables, respectively.

263 An automatic algorithm Python Surrogate Optimization Toolbox (pySOT) developed by
 264 Eriksson et al. (2017) was adopted for the multiple-objective optimization. The pySOT
 265 algorithm used a surrogate model to guide the search for improved solutions, with the advantage
 266 of needing few function evaluations to find a good solution. In each pySOT running, the
 267 optimization procedure was stopped if a maximum number of allowed function evaluations was
 268 reached, which was set as 3000 in this study. For the bi- and tri-objective calibrations,
 269 $0.5 \cdot (NSE_{\text{dis}} + NSE_{\text{Indis}}) - RMSE_{\text{SCA}}$ and $0.5 \cdot (NSE_{\text{dis}} + NSE_{\text{Indis}}) - RMSE_{\text{SCA}} + NSE_{\text{iso}}$ were chosen as
 270 the combined optimization objectives. For each scenario, the pySOT algorithm was repeated
 271 100 times, and behavioral parameter sets were selected among the 100 final results according
 272 to the performance metric thresholds, i.e., only the parameter sets producing metrics better than
 273 certain threshold values were regarded as behavioral parameter sets. The model uncertainty was
 274 evaluated based on the model performance driven by the behavioral parameter sets. The
 275 threshold values of evaluation metrics were used as $0.5 \cdot (NSE_{\text{dis}} + NSE_{\text{Indis}}) > 0.8$, $RMSE_{\text{SCA}} < 0.08$
 276 in the YTR basin; and $NSE_{\text{dis}} > 0.7$, $RMSE_{\text{SCA}} < 0.15$ in the KR catchment. Different values were
 277 adopted for the NSE_{iso} threshold among different scenarios, which would be introduced in the
 278 Result section.

279 **[Table 2]**

280 **2.4 Numerical experiments**

281 The influences of isotope data conditions on model performance were evaluated in three
 282 aspects as listed in Table 3: the assumed glacier meltwater isotope composition, the site
 283 measurement of precipitation isotope for data merging, and the stream water sampling strategy
 284 for model calibration.

285 **[Table 3]**

286 *Experiment 1: influence of assumed glacier meltwater isotope*

287 The first experiment was designed to test the reliance of model performance on the
 288 assumed glacier meltwater isotope, as glacier melt water samples are typically not available for
 289 isotope analysis in high mountain basins on the TP. In this experiment, variable glacier melt

290 isotope signatures were adopted to calculate the isotopic contribution from glacier meltwater to
291 streamflow, assuming the glacier meltwater $\delta^{18}\text{O}$ is 1‰, 3‰, 7‰ and 9‰ (i.e., $\Delta\delta$ values in
292 Table 3) lower than the long-term average $\delta^{18}\text{O}$ of precipitation. A benchmark model running
293 by the literature based $\Delta\delta$ value of 5‰ was used as a baseline reference to assess the influence
294 of the assumed glacier meltwater isotope on the model performance.

295 *Experiment 2: influence of site measurement of precipitation isotope*

296 The second experiment was designed to test the reliance of the model performance on the
297 availability of measured site precipitation isotope that was merged with the isoGSM product.
298 The benchmark model running was forced by the merging precipitation isotope data based on
299 measurements of precipitation isotope from all the four sampling sites (Figure 1). Three
300 scenarios regarding the availability of measured precipitation isotope were designed as shown
301 in Table 3. First, we assumed that only precipitation isotope measured at the two downstream
302 sites of Nuxia and Yangcun are available for data merging (i.e., scenario P_2stationNY in Table
303 3). Second, we assumed that precipitation isotope measurement at the most upstream site Lazi
304 is available. In addition to the measurement at the downstream site Nuxia (i.e., scenario
305 P_2stationNL in Table 3). Third, we assumed that only precipitation isotope measurement at
306 the most downstream site Nuxia is available for the data merging (i.e., scenario P_1station in
307 Table 3).

308 *Experiment 3: influence of stream water sampling strategy*

309 The third experiment was conducted to analyze the influence of stream water sampling
310 strategy on the model performance. Two types of stream water sampling strategies were
311 considered, i.e., a time series sampling strategy based on regular and continuous sampling work
312 at a certain point, and a spatially distributed sampling strategy based on one-time field
313 campaigns of sampling work. For the time series sampling strategy, 7 scenarios (“RT_YTR_”
314 scenarios in Table 3) were designed to analyze the influences of the sampling frequency, the
315 duration of the sampling period, and the number of sampling sites. For the spatially distributed
316 sampling strategy, two scenarios (Figure 1b) were designed to represent typical field campaign
317 activities: collecting samples along the mainstream of the basin (RS_YTR_Main, Table 3), and
318 collecting water samples additionally from major tributaries (RS_YTR_Tributary, Table 3).
319 Considering the limited availability of stream water $\delta^{18}\text{O}$ measurement in the YTR basin (only
320 wet season in one year, Table 1), a supplementary experiment was designed to test the influence
321 of sampling period duration on the model performance using the relatively long time-series
322 isotope dataset in the small catchment KR (“RT_KR_” scenarios in Table 3).

323 To evaluate the influence of isotope data availability on the model performance, we carried
324 out benchmark model simulations forced by full datasets of input isotope and stream water
325 isotope data in the YTR and KR catchments (Table 3). The benchmark model runs were

326 calibrated by a bi-objective calibration using SCA and streamflow observations, and a tri-
 327 objective calibration using additional stream water isotope, respectively. It is noted that, in the
 328 scenarios of experiment 3 in YTR basin (i.e., “RT_YTR_” and “RS_YTR_” scenarios in Table
 329 3), the assumed data availability was beyond the actual measurement dataset. Consequently,
 330 the assumed stream water $\delta^{18}\text{O}$ measurement data were obtained from a model simulation
 331 driven by a benchmark parameter set (rather than a subset of actual measurement stream water
 332 $\delta^{18}\text{O}$), which was selected from the behavioral parameters of the BM_YTR scenario calibrated
 333 by the tri-objective approach. The influence of the availability of stream water $\delta^{18}\text{O}$
 334 measurement on the tracer-aided model were evaluated by comparing the estimated CRCs and
 335 corresponding uncertainties with the assumed true values that were derived from the tri-
 336 objective calibrated benchmark running. Mean absolute error (MAE) and standard deviation
 337 (STD) were used to quantify the accuracy and uncertainty of CRC, which were calculated in
 338 Eqs. 9 and 10.

$$339 \quad \text{MAE}^k = \frac{\sum_{i=1}^n |\text{CRC}_{s,i}^k - \text{CRC}_o^k|}{n} \quad (9)$$

$$340 \quad \text{STD}^k = \sqrt{\frac{\sum_{i=1}^n (\text{CRC}_{s,i}^k - \overline{\text{CRC}_s^k})^2}{n}} \quad (10)$$

341 where, n is the number of behavioral parameter sets, and superscript k indicates the runoff
 342 component (one of rainfall, snowmelt, glacier melt and baseflow). Subscript s and o indicate
 343 the simulated and observed value (observed value is the CRC produced by the tri-objective
 344 calibrated benchmark running). $\text{CRC}_{s,i}^k$ is the contribution of runoff component k simulated by
 345 the parameter set i . $\overline{\text{CRC}_s^k}$ is the average CRC simulated by all the behavioral parameter sets.

346 In the scenarios of experiments 1 and 2, the model was calibrated towards the complete
 347 stream water $\delta^{18}\text{O}$ measurement dataset (Table 1), and the influence of isotope data availability
 348 on model performance were quantified by changes in model performance in the validation
 349 period and internal validate hydrological stations, as well as the uncertainty of CRC estimated
 350 by Eq. 10. In the scenarios of experiment 3 in the KR catchment (i.e., “RT_KR_” scenarios in
 351 Table 3), subsets of stream water $\delta^{18}\text{O}$ measurement dataset (Table 1) with different length were
 352 picked out for model calibration.

353 **3. Results**

354 **3.1 Performance of the tracer-aided hydrological model**

355 Figure 2 shows performance of the benchmark model running (i.e., BM_YTR scenario in
 356 Table 3) forced and calibrated by the full available isotope dataset. The NSE_{iso} threshold by
 357 which behavioral parameter sets were selected in tri-objective calibration was set as 0.5.
 358 Seasonal variations in discharge and SCA were reproduced well by the bi-objective calibration
 359 (Figure 2a and 2b), indicated by the high values of NSE_{dis} (>0.8) and $\ln\text{NSE}_{\text{dis}}$ (>0.8), and a low

360 RMSE_{SCA} (<0.08). The peak flows were less well reproduced by the model in comparison to
361 the simulation of baseflow processes, partly due to the inaccurate precipitation input data at the
362 high altitudes. The model showed extremely poor performance for the simulation of stream
363 water isotope when looking at the large uncertainty range (Figure 2c) and low NSE_{iso} (-0.72).
364 The tri-objective calibration significantly improved the isotope simulation (Figure 2f), without
365 bringing much sacrifice to the performance in simulating discharge and SCA (considering the
366 minimum values of NSE_{dis} and lnNSE_{dis} are around 0.7 in Figure 2d and 2e). Moreover, the tri-
367 objective calibration slightly reduced uncertainty for simulation of the rising hydrograph in the
368 2009 spring (Figure 2d). The seasonal variations in stream water $\delta^{18}\text{O}$ were captured well at all
369 the four stations by simulations from the tri-objective calibration. The mean contributions of
370 rainfall and snowmelt to annual streamflow estimated by the bi-objective calibration were 62.8%
371 and 10.8%, which were around 1%-7% smaller than those estimated by the tri-objective
372 calibration (Table 4). In contrast, the contribution of glacier melt estimated by the tri-objective
373 calibration (17.1%) was lower than that estimated by the bi-objective calibration (26.4%).
374 Surface runoff which was mainly fed by glacier melt in the YTR showed a larger proportion in
375 the total streamflow simulated by a bi-objective calibration (52.1%) than that in the simulation
376 of a tri-objective calibration (44.7%), while baseflow contribution quantified by the bi-
377 objective calibration is smaller. Standard deviation values of the quantified CRCs indicated that
378 the tri-objective calibration estimated smaller uncertainties for the quantifications of runoff
379 components.

380 **[Figure 2]**

381 **[Table 4]**

382 The uncertainties of behavioral parameter set obtained by bi- and tri-objective calibration
383 are shown in Figure 3. Apart from the hillslope roughness coefficient (nt), the uncertainties of
384 all the parameters were reduced by tri-objective calibration, especially the parameters related
385 to melting (DDF_N and T_o) and flow concentration processes ($C1$ and $C2$). The higher melting
386 temperature threshold (T_o) obtained by tri-objective calibration was consistent with the lower
387 contribution of melting water. The lower water storage capacity (WM) and higher shape
388 coefficient (B) of tri-objective calibration should result in higher saturation area and
389 consequently higher contribution of surface runoff, which was however not in agreement with
390 the estimated CRC, indicating the important contribution of glacier melt in surface runoff. A
391 benchmark parameter set that performed well on multiple objectives was selected among the
392 behavioral parameters of BM_YTR calibrated by tri-objective method (as shown in Table 5),
393 to produce stream water $\delta^{18}\text{O}$ for model calibration in experiment 3 in YTR basin. It is noted
394 that this benchmark parameter set was only used to produce stream water $\delta^{18}\text{O}$ data for model
395 calibration in experiment 3 in YTR basin, not an optimal parameter set representing the true
396 hydrological processes.

397

[Figure 3]

398

[Table 5]

399

400 Figure 4 shows model performances in the KR catchment. The parameter sets producing
401 positive NSE_{iso} were selected as behavioral for tri-objective calibration. Variations of discharge
402 and SCA were reproduced comparably well by the bi- and tri-objective calibrations indicated
403 by the similar metric values. However, the bi-objective calibration produced extremely poor
404 performance for the isotope simulation with low NSE_{iso} and a large simulation error of $\sim 5\%$
405 (Figure 4c). The tri-objective calibration captured the seasonal variations in stream water $\delta^{18}O$
406 during the study period well. Similarly to YTR, the tri-objective calibration resulted in lower
407 uncertainty in the simulated hydrograph (e.g., early 2010, 2006 and 2008), benefiting from
408 involving isotope for the model calibration to reject parameter sets that produced good
409 performance for discharge and SCA simulations but poor performance for isotope simulation.
410 Regarding the CRCs to total streamflow, the bi-objective and tri-objective calibrations
411 estimated similar results with differences up to 3%. The mean contributions of rainfall,
412 snowmelt and glacier melt to annual streamflow in the KR catchment were around 45%, 22%
413 and 33%, respectively. Contribution of surface runoff estimated by the bi-objective calibration,
414 however, was 13% lower than that estimated by the tri-objective calibration. In contrast,
415 baseflow is more important in the total streamflow simulated by the bi-objective calibration
416 (accounting for 38%) in comparison to the simulation of the tri-objective calibration
417 (accounting for 25%). Again in the KR catchment, uncertainties of CRCs quantified by the tri-
418 objective calibration are much smaller than those estimated by the bi-objective calibration
419 (Table 4).

419

[Figure 4]

420 3.2 Changes in model simulations forced by different assumed glacier meltwater isotopes

421 Behavioral parameter sets of experiment 1 were selected based on the same NSE_{iso}
422 threshold (0.5) with the benchmark running. Model simulations forced by assumed glacier
423 meltwater $\delta^{18}O$ that are 5‰ (scenario BM_YTR, $\Delta\delta=5\%$) and 7‰ (scenario G_Δ7, $\Delta\delta=7\%$)
424 lower than the long-term average precipitation $\delta^{18}O$ showed the best discharge simulations in
425 the validation period (2011-2015) and stations (Yangcun and Nugesha), indicated by the high
426 average metric values (Figure 5a-d). It is noted that simulations of all the glacier meltwater
427 isotope input scenarios in experiment 1 except G_Δ1 performed better than the bi-objective
428 calibration in which isotope data was not involved for parameter identification. Discharge
429 simulation in the scenario of G_Δ1 estimated higher performance in the validation period than
430 the bi-objective calibration (Figure 5a), but lower performance at internal stations (Figure 5b
431 and 5c).

432

[Figure 5]

433 Figure 5 (e-h) shows the average CRCs and corresponding uncertainties estimated by the
434 different glacier melt isotope inputs. Scenarios with larger $\Delta\delta$ values (i.e., glacier meltwater
435 isotope is much lower than precipitation isotope) tended to result in higher contributions of
436 precipitation and lower contributions of glacier melt. This can be expected, as stream water
437 $\delta^{18}\text{O}$ is a mixture mainly from $\delta^{18}\text{O}$ of precipitation and glacier meltwater in YTR basin and
438 precipitation $\delta^{18}\text{O}$ is fixed in all the scenarios. Result of scenario G_Δ1, however, estimated a
439 smaller contribution of glacier melt than the scenario G_Δ3. This was likely due to that the
440 behavioral parameter sets were selected based on the performance of both discharge and isotope
441 simulations. Parameter sets that estimated higher glacier melt contribution with good
442 performance in isotope simulation but performed poorly on discharge simulation were excluded
443 from the behavioral set in the G_Δ1 scenario.

444 **3.3 Changes in model performance forced by isoGSM product merged with different site** 445 **measurements of precipitation isotope**

446 Figure 6 shows the relationship between REW-scale weighted averages of precipitation
447 $\delta^{18}\text{O}$ and the longitude/elevation of corresponding REW for the scenarios in experiment 2. The
448 precipitation $\delta^{18}\text{O}$ showed similar spatial pattern in the scenarios merging isoGSM with
449 measurement data at more than one sites. In scenario P_1station that isoGSM was merged
450 with measurement data only at the most downstream station Nuxia, however, spatial pattern
451 was different, showing significantly higher precipitation $\delta^{18}\text{O}$ than other scenarios. The
452 different precipitation $\delta^{18}\text{O}$ pattern was mainly a result of different altitudinal lapse rates of the
453 isoGSM bias (i.e., parameter a in equation 2). Representing the bias characteristic in the whole
454 basin solely by the data measured at the most downstream station resulted in significantly
455 smaller isoGSM bias, and consequently overestimated precipitation $\delta^{18}\text{O}$.

456 Different precipitation $\delta^{18}\text{O}$ input data inevitably resulted in different simulations of stream
457 water $\delta^{18}\text{O}$ as shown in Figure 7. The NSE_{iso} threshold was set as 0.5 except for scenario
458 P_1station, which produced extremely poor $\delta^{18}\text{O}$ simulation due to the high bias in precipitation
459 $\delta^{18}\text{O}$ input data (Figure 7d). The other three scenarios all performed well in stream $\delta^{18}\text{O}$
460 simulation (Figure 7a-c), among which scenario P_2stationNL produced highest behavior,
461 followed by P_4station and P_2stationNY.

462 **[Figure 6]**

463 **[Figure 7]**

464 Different precipitation isotope input data also led to different performance in hydrological
465 modeling (Figure 8a-d). While different scenarios produced similar SCA simulations in the
466 validation period (Figure 8d), the performance of discharge simulation significantly differed
467 among the precipitation isotope input scenarios. In scenarios BM_YTR and P_2stationNL, the
468 model performed better than the bi-objective calibration in the validation period (Figure 8a)

469 and stations (Figure 8b and 8c), showing higher average values and smaller ranges of NSE_{dis} ,
470 which indicated that the model benefitted from involving isotope data for calibration. The
471 model performance forced by scenario P_2stationNY was close to that of the bi-objective
472 calibration, with poorer discharge simulation at internal stations (Figure 8b and 8c). Using
473 precipitation isotope input from the scenario P_1station, however, the model performance was
474 significantly worse than that of the bi-objective calibration. Reasons for the variable model
475 performance forced by the precipitation isotope input scenarios could be: Site measurements of
476 precipitation isotope used in scenarios BM_YTR (using data at four sampling stations) and
477 P_2stationNL (using data at the most downstream sampling station and the most upstream
478 sampling station) tended to provide more informative spatial distribution of precipitation $\delta^{18}O$
479 in the basin and were the most valuable data for the precipitation isotope data merging; in the
480 scenario of P_1station, on the contrary, the bias of isoGSM product was inadequately corrected
481 by site precipitation isotope measured only at the most downstream station Nuxia, resulting in
482 much errors in the isoGSM product at high altitudes. Although precipitation isotope input data
483 did not influence the simulation of hydrological processes, the calibration process that
484 attempted to match simulated stream $\delta^{18}O$ with measurement influenced the parameter and
485 consequently affected the internal hydrological processes.

486 [Figure 8]

487 Figure 8 (e-h) shows the average CRCs and corresponding uncertainties estimated by the
488 different precipitation isotope input scenarios. All scenarios produced lower uncertainties than
489 the bi-objective calibration, which can be expected as they were calibrated by a tri-objective
490 approach. The variable precipitation input scenarios resulted in contribution differences of
491 around 10% in runoff components of rainfall, glacier melt and baseflow. The sort of estimated
492 contribution of rainfall (P_2stationNL > BM_YTR > P_2stationNY > P_1station) was opposite
493 to that of average precipitation $\delta^{18}O$ shown in Figure 6, which was consistent with the
494 estimation based on the end-member mixing method.

495 Among the evaluation metrics, discharge simulation at Nugesha station showed the largest
496 sensitivity to precipitation isotope inputs. As shown in Figure 9, scenarios P_2stationNY and
497 P_1station estimated higher contribution of meltwater, earlier discharge onset timing and higher
498 peak flow. The discharge began to rise especially early (around February) in scenario P_1station,
499 because of the low calibrated value for the melting temperature threshold T_0 (-4.5°C), resulted
500 in extremely poor discharge simulation (average NSE is around 0, Figure 9d).

501 [Figure 9]

502 3.4 Model performance constrained by different stream water sampling strategies

503 Figure 10 shows the accuracy and uncertainty metrics of CRCs produced by experiment 3
504 in the YTR basin. The NSE_{iso} threshold was set as 0.8, because the stream isotope data for

505 model calibration was generated by a benchmark parameter set, towards which good simulation
506 was rather easy to produce. In comparison to the baseline scenario of RT_TYR_BM, collecting
507 stream isotope data in the dry season (i.e., from November to next February in scenario
508 RT_YTR_WholeYear) brought little benefits to the estimation of water sources proportions, but
509 significantly improved the quantifications of runoff generation pathways indicated by the lower
510 MAE and STD in Figure 10b. The stream water in dry season was fed mainly by groundwater.
511 Stream water isotope data collected in this period reflect the release of groundwater storage,
512 thus helping to constrain the partition between surface and subsurface runoff pathway. On the
513 other hand, reducing the frequency of stream isotope data from weekly to monthly (i.e., scenario
514 RT_YTR_Monthly) led to significantly higher MAE and STD for both the partitions of water
515 sources and runoff pathways, which indicated that stream water isotope data collected by a
516 monthly sampling strategy could provide less constrains to model calibration. Extending the
517 duration of stream isotope sampling period by one or two years (i.e., scenarios RT_YTR_2year
518 and RT_YTR_3year) did not bring much benefits to the quantifications of CRCs regarding the
519 similar metric values. Using stream water isotope data from a three years' sampling
520 (RT_YTR_3year) even led to higher MAE and STD than that using stream water isotope data
521 from a 2 years' sampling (RT_YTR_2year), which might be an occasional result obtained by
522 the random calibration procedure (100 pySOT runs). In comparison to simulations constrained
523 by stream water isotope data from multiple sampling years, results constrained by stream water
524 isotope data from multiple sampling sits (i.e., scenarios of RT_YTR_2station and
525 RT_YTR_4station) yielded lower MAE and STD for the quantified CRCs.

526 [Figure 10]

527 Model simulations calibrated by spatially distributed stream $\delta^{18}\text{O}$ data collected in a one-
528 time field campaign reduced the CRC uncertainty compared to the bi-objective calibration
529 (Figure 10). However, its MAE and STD for the quantifications of CRCs were higher than that
530 estimated by the model when calibrated by weekly sampled time series of stream $\delta^{18}\text{O}$.
531 Additionally using stream isotope data from four major tributaries (i.e., scenario
532 RS_YTR_Tributary) brought little benefits to the model performance than using isotope data
533 from the main stream solely (RS_YTR_Main), partly due to the signatures of stream water
534 isotope from tributaries were already reflected by water samples collected at confluences on
535 the main river channel.

536 In the KR catchment, stream isotope data was collected from five continues years,
537 providing better data basis for the evaluation of the influence of sampling period duration. The
538 NSE_{iso} threshold was set as 0, same with the benchmark scenario in KR catchment. Figure 11
539 compares the CRC estimations and their uncertainty metric STD of variable scenarios. For the
540 estimate of water sources, the model produced rather large uncertainty ranges of ~20% and ~40%
541 for the contributions of rainfall and glacier melt when calibrating the model using discharge

542 and SCA. Using one-year's stream water isotope data for model calibration, the uncertainty
543 ranges were reduced by rejecting some outliers as shown in Figure 11a-c, but the STD was still
544 large (Figure 11e). The STD can be reduced by increasing the number of calibration isotope
545 data at a rate of ~1%/year. Using isotope data collected from five years, however, didn't result
546 in further decrease in the CRC uncertainties compared to the result calibrated by isotope data
547 collected in a four-year sampling period. The situation, however, was quite different for the
548 estimates of runoff pathways. The bi-objective calibration produced a large uncertainty of ~40%
549 and a STD of ~10% (Figure 11d) for the contribution of baseflow. Using one-year's data for
550 model calibration, the uncertainty range was significantly reduced by about half of that
551 modelled by the bi-objective calibration (from ~10% to ~5%). However, further increase in the
552 duration of sampling period did not bring much improvements on constraining the uncertainties
553 in quantifications of runoff pathways with STD fluctuating around only 4%. It is indicated that
554 model calibration upon more stream isotope data was useful to better constrain the uncertainties
555 of the model simulations and modeled CRCs, but benefit would disappear after a certain
556 duration of stream water sampling period has been reached.

557 **[Figure 11]**

558 **4. Discussions**

559 **4.1 Implications for water sampling for isotope analysis in high mountains of TP**

560 This study tested the reliance of the benefits of using tracer-aided hydrological model on
561 isotope data availability in two mountainous catchments YTR and KR on the TP. Our findings
562 consistently showed that the model robustness, with respect to performance in the validation
563 period and internal stations and the quantifications of CRCs, can be significantly improved by
564 involving isotope data for parameter calibration, similarly to previous tracer-aided modeling
565 studies (e.g., He et al., 2019; Ala-aho et al., 2017; Birkel et al., 2010). It can be expected that
566 more data help to provide more constrains on identification of model parameters. Nonetheless,
567 water sampling in high mountains on the TP is restricted by environment accessibility, financial
568 and human costs (Stevenson et al., 2021, Li et al., 2020). It is therefore highly needed to find
569 optimal strategies of collecting water samples that balance well between data adequacy for
570 model running and affordable sampling cost (Sprenger et al., 2019).

571 As an important water source in mountainous catchment on the TP, sampling of glacier
572 meltwater was expected to be favorable for the determination of glacier meltwater isotopic
573 composition and its contribution to total streamflow (He et al., 2019). Field campaign for
574 sampling of glacier melt water is strongly challenging in the YTR basin in this study, due to the
575 harsh accessibility of very high altitudes where glaciers lie. We thus assumed that glacier
576 meltwater $\delta^{18}\text{O}$ was lower than the average local precipitation $\delta^{18}\text{O}$ by an offset parameter ($\Delta\delta$).

577 This simple assumption turned to work well on driving the tracer-aided hydrological model and
578 produced better performance than the bi-objective calibration in both validation periods and
579 internal stations. Experiments by using different $\Delta\delta$ values indicated that the prior assumed
580 isotopic compositions of glacier melt have small influence on the estimated glacier meltwater
581 contribution in the YTR basin. It should be noted that this was different from the results of some
582 hydrograph separation works (e.g., Pu et al., 2020; Lone et al., 2021), which indicated important
583 influence of meltwater isotope composition in estimating the CRC. Those works were based on
584 the end-member mixing approach, which was applied in a short time scale, and was more
585 dependent on the isotope composition of each runoff component. However, this study applied
586 the tracer-aided hydrological model in a longer time scale, where the temporal variability of
587 isotope composition played a more important role than its absolute value, on the parameter
588 calibration. Consequently, when the temporal variabilities of isotope composition of each water
589 source were reproduced properly, the glacier melt $\delta^{18}\text{O}$ value in a reasonable range would have
590 little influence on the model performance. The $\Delta\delta$ values ranging from 2‰-9‰ led to only ~5%
591 difference in the estimated contributions of glacier melt. Using a $\Delta\delta$ to estimate glacier
592 meltwater $\delta^{18}\text{O}$ could serve as an option to force the tracer-aided hydrological models in high-
593 mountain catchments where collecting glacier meltwater samples is highly challenging.

594 Results of experiment 2 indicated that the original isoGSM precipitation $\delta^{18}\text{O}$ data showed
595 large bias in the high mountain basins on TP, and must be corrected by or merged with
596 measurement data before using to force the tracer-aided hydrological model. Our experiments
597 showed that measurement of precipitation isotope at only two sampling sites (scenario
598 P_2stationNL) in the large YTR basin of $2 \times 10^5 \text{ km}^2$ can be highly valuable for isotope data
599 merging. Forced by isoGSM data that was merged with precipitation $\delta^{18}\text{O}$ measurements from
600 two sampling sites, the model performed better than the bi-objective calibration in simulating
601 discharge in the validation period and internal stations, and performed comparably to the
602 simulations of a benchmark running which used precipitation $\delta^{18}\text{O}$ measurements from four
603 stations for the data merging. This benefitted from the large altitudinal range covered by the
604 two sampling sites (a most downstream site Nuxia and a most upstream site Lazi) to represent
605 the spatial pattern of isoGSM bias. Likewise using measurement data at two sites in the scenario
606 P_2stationNY, model performance deteriorated visibly, as the sampling sites (Nuxia and
607 Yangchun) were both located in the downstream regions, being worse at representing the spatial
608 pattern of precipitation $\delta^{18}\text{O}$ over the basin. Consequently, the strategy of collecting
609 precipitation samples for isotope data merging should be carefully designed; spending high cost
610 on collecting precipitation samples within a small region might be not worth at improving the
611 performance of the tracer-aided hydrological model.

612 Measurements of stream water $\delta^{18}\text{O}$ are essential for the calibration and evaluation of
613 tracer-aided hydrological models. Three kinds of sampling strategies in YTR basin were

614 evaluated in experiment 3: one-time campaign field sampling, continuous sampling at a fixed
615 location for a long period, and continuous sampling at multiple fixed locations during a short
616 period. It is indicated that continuously sampled stream water $\delta^{18}\text{O}$ at a fix location is more
617 valuable for aiding hydrological model than that collected by one-time field sampling
618 campaigns at distributed sites. Seasonality of stream water $\delta^{18}\text{O}$ referring to the processes of
619 water storage, mixture and transport in the basin can be better captured by continuous time
620 series measurements of $\delta^{18}\text{O}$ data (McGuire and McDonnell, 2006). Spatially sampled stream
621 water $\delta^{18}\text{O}$ data by one-time field sampling campaigns possibly miss seasonal $\delta^{18}\text{O}$ signatures
622 of stream water that were caused by seasonal runoff generation processes (Kendall and Coplen,
623 2001; Nan et al., 2019), and provide less constrains for the model calibration. Sampling of
624 stream water during dry season (scenario RT_YTR_WholeYear) brought little improvements
625 to the modeling of water source proportions, which is consistent with the findings in Stevenson
626 et al. (2021). High frequent like weekly sampling of stream water in the dry season makes small
627 senses on improving the stream $\delta^{18}\text{O}$ data quality, as stream $\delta^{18}\text{O}$ in this season has little
628 variations due to small precipitation triggered runoff inputs. Monthly sampling of stream water
629 (RT_YTR_Monthly) turned to be insufficient to capture the strong hydrological variations in
630 the wet season (Birkel and Soulsby, 2015). For large basins like YTR, increasing the number
631 of sampling site for stream water $\delta^{18}\text{O}$ is more useful than extending the years of sampling
632 period at fixed sites, as seasonality of $\delta^{18}\text{O}$ signatures of water sources should be similar among
633 years in a short study period. Consequently, continuous sampling at multiple locations in a short
634 period like one or two years seems to be the optimal stream sampling strategy for running
635 tracer-aided hydrological model in mountainous basins like YTR on the TP. The value of
636 extending sampling period was more significant in a smaller catchment KR. The uncertainty of
637 CRC estimation kept decreasing until the data series length reached four years and two years,
638 for the aspects of water source and runoff pathway, respectively. This was consistent with the
639 finding by Stevenson et al. (2021) that the benefits from isotope plateaued after a certain year
640 number, which was five for that study.

641 **4.2 Uncertainties and limitations**

642 This study used simulated stream $\delta^{18}\text{O}$ of a benchmark model running to represent the fully
643 available dataset of stream $\delta^{18}\text{O}$ for water sampling in the YTR basin, due to the limited stream
644 water samples. This procedure likely caused the inherent correlation of the stream $\delta^{18}\text{O}$ dataset,
645 which made the model easily reproduce the assumed measurements of stream $\delta^{18}\text{O}$ and may
646 underestimate the value of stream $\delta^{18}\text{O}$ data collected in extended sampling years and sampling
647 sites. Results in this study serve to provide preliminary understandings of the influences of
648 stream water sampling strategy on the model performance. More solid evaluations, however,
649 can be further benefited from using more real field measurements of stream $\delta^{18}\text{O}$ in the

650 mountain basins.

651 Our study tried to look for optimal water sampling strategies to provide isotope input and
652 calibration data for the tracer-aided hydrological model in the YTR basin and KR catchment on
653 the TP. The transferability of our findings to other basins can be partly expected. For example,
654 we can expect that in catchments where precipitation $\delta^{18}\text{O}$ and runoff processes show small
655 spatial heterogeneity, collecting water samples at multiple stations would bring few additional
656 benefits for the modeling work than collecting water samples at a sole station. The influence of
657 assumed glacier meltwater would differ with the glacier covered area fraction in the basins.
658 However, situations in catchments with different geographical and climatic characteristics were
659 not evaluated in this study, which is restricted by the fact that high-quality water isotope data
660 in a set of mountain basins on the TP were hardly available currently (Birkel and Soulsby, 2015).
661 The authors suggest tracer-aided modeling researchers to publish their water isotope data to
662 improve the evaluation of the reliance of tracer-aided modeling performance on water sampling
663 strategy (similarly to He et al. 2021; Niinikoski et al., 2016; Yde et al., 2016).

664 The model performances were evaluated based on the behavioral parameter sets, which
665 were selected by the threshold values of evaluation metrics. The threshold values were
666 determined by looking at the graph comparing simulation and observation values, and
667 artificially judging whether good fitness has been achieved. This process was rather subjective
668 and had inevitable influence on the evaluation result. However, this was a widely used method
669 (e.g., Birkel et al., 2011; Delavau et al., 2017; He et al., 2019), and the threshold values were
670 set at levels achieved by the studies conducted in the same region (e.g., Zhang et al., 2015;
671 Chen et al., 2017).

672 **5. Conclusion**

673 The value of water isotope data for aiding hydrological modeling in large mountainous
674 catchments was tested by a set of numerical experiments in the YTR basin. Reliance of the
675 tracer-aided model performance on the availability of input isotope data and evaluation stream
676 water isotope data was extensively investigated in the numerical experiments. Results could
677 provide important guidance for collecting water samples and establishing tracer-aided
678 hydrological model in mountainous regions on the TP. Our main finds are as follows:

679 1. In high-mountain basins where glacier meltwater samples for isotope analysis are not
680 available, estimating isotopic composition of glacier meltwater by an offset parameter from
681 precipitation isotope is a feasible way to force the tracer-aided hydrological model. Our test
682 indicated that using a set of glacier meltwater $\delta^{18}\text{O}$ that are 2‰~9‰ lower than the mean
683 precipitation $\delta^{18}\text{O}$, resulted in small changes in the model performance and the quantifications
684 of CRCs (smaller than 5%) in the YTR basin. This influence, however, is expected to change
685 with the glacier area coverages in other mountain basins.

686 2. Strategy of field sampling for precipitation to collect measurement precipitation $\delta^{18}\text{O}$
687 merged with isoGSM product should be carefully designed. Collecting precipitation samples at
688 sites from the same altitude tends to be worse at representing the spatial pattern of precipitation
689 $\delta^{18}\text{O}$ over the basin than collecting precipitation samples from sites covering a range of altitudes.
690 Measurements of precipitation isotope at only two sampling sites covering an elevation range
691 of 2900-6900m in the large YTR basin of $2 \times 10^5 \text{ km}^2$ can be highly valuable for precipitation
692 isotope data merging.

693 3. Collecting weekly stream water samples at multiple sites in the wet and warm seasons is
694 the optimal strategy to capture more hydrological process variability for calibrating and
695 evaluating a tracer-aided hydrological model in the YTR basin. It is highly recommended to
696 increase the number of stream water sampling sites in the high-mountain basins rather than
697 extending the duration of sampling period at a sole site. Benefits from extending the duration
698 of sampling period is more visible in a small catchment but smaller in large basins, and tend to
699 disappear when a certain duration of sampling period has been reached.

700

701 **Code and data availability**

702 Code and data availability. The isotope data and the code of THREW-T model used in this study
703 are available from the corresponding author (tianfq@tsinghua.edu.cn). Other data sets and the
704 calibration program pySOT are publicly available as follows: DEM
705 (<http://www.gscloud.cn/sources/details/310?pid=302>, last access: 1 January 2019, Geospatial
706 Data Cloud Site, 2019), CMFD (<https://doi.org/10.11888/AtmosphericPhysics.tpe.249369.file>,
707 Yang and He, 2019), glacier data (<https://doi.org/10.3972/glacier.001.2013.db>, Liu et al., 2012),
708 NDVI (<https://doi.org/10.5067/MODIS/MOD13A3.006>, Didan et al., 2015), LAI
709 (<https://doi.org/10.5067/MODIS/MOD15A2H.006>, Myneni et al., 2015), HWSD
710 (<https://data.tpdc.ac.cn/zh-hans/data/3519536a-d1e7-4ba1-8481-6a0b56637baf/?q=HWSD>,
711 last access: 1 January 2019, He, 2019) and the pySOT program
712 (<https://doi.org/10.5281/zenodo.569554>, Eriksson et al., 2017). These data sets and programs
713 are also referred to in the main text (Yang et al., 2010; Chen et al., 2018).

714 **Author contribution**

715 YN, ZH and FT conceived the idea; ZW provided the isoGSM data; LT provided the
716 measurement isotope data; YN, ZH and FT conducted analysis; ZW and LT provided comments
717 on the analysis; all the authors contributed to writing and revisions.

718 **Financial support**

719 This study has been supported by the National Natural Science Foundation of China (grant no.
720 92047301 and 51879136) and the Shuimu Tsinghua Scholar Program.

721 **Competing interests**

722 At least one of the (co-)authors is a member of the editorial board of Hydrology and Earth
723 System Sciences.

724

725 **References**

726 Ala-aho, P., Tetzlaff, D., McNamara, J. P., Laudon, H., and Soulsby, C.: Using isotopes to
727 constrain water flux and age estimates in snow-influenced catchments using the STARR
728 (Spatially distributed Tracer-Aided Rainfall–Runoff) model, *Hydrology and Earth System*
729 *Sciences*, 21, 5089-5110, 10.5194/hess-21-5089-2017, 2017.

730 Birkel, C., Dunn, S. M., Tetzlaff, D., and Soulsby, C.: Assessing the value of high-resolution
731 isotope tracer data in the stepwise development of a lumped conceptual rainfall-runoff
732 model, *Hydrological Processes*, 24, 2335-2348, 10.1002/hyp.7763, 2010.

733 Birkel, C., Tetzlaff, D., Dunn, S. M., and Soulsby, C.: Using time domain and geographic source
734 tracers to conceptualize streamflow generation processes in lumped rainfall-runoff models,
735 *Water Resources Research*, 47, 10.1029/2010wr009547, 2011.

736 Birkel, C., and Soulsby, C.: Advancing tracer-aided rainfall-runoff modelling: a review of
737 progress, problems and realized potential, *Hydrological Processes*, 29, 5227-5240,
738 10.1002/hyp.10594, 2015.

739 Bloeschl, G., and Montanari, A.: Climate change impact: throwing the dice?, *Hydrological*
740 *Processes*, n/a-n/a, 10.1002/hyp.7574, 2009.

741 Boral, S., and Sen, I. S.: Tracing ‘Third Pole’ ice meltwater contribution to the Himalayan rivers
742 using oxygen and hydrogen isotopes, *Geochemical Perspectives Letters*, 48-53,
743 10.7185/geochemlet.2013, 2020.

744 Bowen, G. J., Cai, Z., Fiorella, R. P., and Putman, A. L.: Isotopes in the Water Cycle: Regional-
745 to Global-Scale Patterns and Applications, in: *Annual Review Of Earth And Planetary*
746 *Sciences*, Vol 47, edited by: Jeanloz, R., and Freeman, K. H., *Annual Review of Earth and*
747 *Planetary Sciences*, 453-+, 2019.

748 Capell, R., Tetzlaff, D., and Soulsby, C.: Can time domain and source area tracers reduce
749 uncertainty in rainfall - runoff models in larger heterogeneous catchments?, *Water*
750 *Resources Research*, 48, 10.1029/2011wr011543, 2012.

751 Chen, X., Long, D., Hong, Y., Zeng, C., and Yan, D.: Improved modeling of snow and glacier
752 melting by a progressive two-stage calibration strategy with GRACE and multisource data:
753 How snow and glacier meltwater contributes to the runoff of the Upper Brahmaputra River
754 basin?, *Water Resources Research*, 53, 2431-2466, 10.1002/2016wr019656, 2017.

755 Chen, X., Long, D., Liang, S., He, L., Zeng, C., Hao, X., and Hong, Y.: Developing a composite
756 daily snow cover extent record over the Tibetan Plateau from 1981 to 2016 using

757 multisource data, *Remote Sen. Environ.*, 215, 284–299,
758 <https://doi.org/10.1016/j.rse.2018.06.021>, 2018.

759 Delavau, C. J., Stadnyk, T., and Holmes, T.: Examining the impacts of precipitation isotope
760 input on distributed, tracer-aided hydrological modelling, *Hydrology and Earth System
761 Sciences*, 21, 2595-2614, 10.5194/hess-21-2595-2017, 2017.

762 Didan, K.: MOD13A3 MODIS/Terra vegetation Indices Monthly L3 Global 1km SIN Grid
763 V006, NASA EOSDIS Land Processes DAAC [data set],
764 <https://doi.org/10.5067/MODIS/MOD13A3.006>, 2015.

765 Dong, G., Weng, B., Chen, J., Yan, D., and Wang, H.: Variation characteristics of stable isotopes
766 in water along main stream of Naqu River in source area of Nujiang River, *Water
767 Resources and Hydropower Engineering*, 49, 108-114, 2018.

768 Duethmann, D., Bolch, T., Farinotti, D., Kriegel, D., Vorogushyn, S., Merz, B., Pieczonka, T.,
769 Jiang, T., Su, B., and Guentner, A.: Attribution of streamflow trends in snow and glacier
770 melt-dominated catchments of the Tarim River, Central Asia, *Water Resources Research*,
771 51, 4727-4750, 10.1002/2014wr016716, 2015.

772 Dunn, S. M., McDonnell, J. J., and Vaché, K. B.: Factors influencing the residence time of
773 catchment waters: A virtual experiment approach, *Water Resources Research*, 43,
774 10.1029/2006wr005393, 2007.

775 Eriksson, D., Bindel, D., and Shoemaker, C.: Dme65/Pysot: V0.1.35, Zenodo [code],
776 <https://doi.org/10.5281/zenodo.569554>, 2017.

777 Gao J., Tian L., and Liu, Y.: Oxygen isotope variation in the water cycle of the Yamzho Lake
778 Basin in southern Tibetan Plateau, *Chinese Sci. Bull.*, 54, 2758–2765, 2009.

779 Gupta, H. V., Wagener, T., and Liu, Y.: Reconciling theory with observations: elements of a
780 diagnostic approach to model evaluation, *Hydrological Processes*, 22, 3802-3813,
781 10.1002/hyp.6989, 2008.

782 He, Y.: Pan-TPE soil map based on Harmonized World Soil Database (V1.2), National Tibetan
783 Plateau Data Center [data set], [https://data.tpdc.ac.cn/zh-hans/data/3519536a-d1e7-4ba1-
784 8481-6a0b56637baf/?q=HWSD](https://data.tpdc.ac.cn/zh-hans/data/3519536a-d1e7-4ba1-8481-6a0b56637baf/?q=HWSD), 2019

785 He, Z. H., Tian, F. Q., Gupta, H. V., Hu, H. C., and Hu, H. P.: Diagnostic calibration of a
786 hydrological model in a mountain area by hydrograph partitioning, *Hydrology and Earth
787 System Sciences*, 19, 1807-1826, 10.5194/hess-19-1807-2015, 2015.

788 He, Z., Unger-Shayesteh, K., Vorogushyn, S., Weise, S. M., Kalashnikova, O., Gafurov, A.,
789 Duethmann, D., Barandun, M., and Merz, B.: Constraining hydrological model parameters
790 using water isotopic compositions in a glacierized basin, Central Asia, *Journal of
791 Hydrology*, 571, 332-348, 10.1016/j.jhydrol.2019.01.048, 2019.

792 He, Z., Unger-Shayesteh, K., Vorogushyn, S., Weise, S. M., Duethmann, D., Kalashnikova, O.,
793 Gafurov, A., and Merz, B.: Comparing Bayesian and traditional end-member mixing

794 approaches for hydrograph separation in a glacierized basin, *Hydrology and Earth System*
795 *Sciences*, 24, 3289-3309, 10.5194/hess-24-3289-2020, 2020.

796 He, Z., Duethmann, D., and Tian, F.: A meta-analysis based review of quantifying the
797 contributions of runoff components to streamflow in glacierized basins, *Journal of*
798 *Hydrology*, 603, 126890, 10.1016/j.jhydrol.2021.126890, 2021.

799 Hindshaw, R. S., Tipper, E. T., Reynolds, B. C., Lemarchand, E., Wiederhold, J. G., Magnusson,
800 J., Bernasconi, S. M., Kretzschmar, R., and Bourdon, B.: Hydrological control of stream
801 water chemistry in a glacial catchment (Damma Glacier, Switzerland), *Chemical Geology*,
802 285, 215-230, 10.1016/j.chemgeo.2011.04.012, 2011.

803 Immerzeel, W. W., van Beek, L. P. H., and Bierkens, M. F. P.: Climate Change Will Affect the
804 Asian Water Towers, *Science*, 328, 1382-1385, 10.1126/science.1183188, 2010.

805 Jeelani, G., Shah, R. A., Jacob, N., and Deshpande, R. D.: Estimation of snow and glacier melt
806 contribution to Liddar stream in a mountainous catchment, western Himalaya: an isotopic
807 approach, *Isotopes in environmental and health studies*, 53, 18-35,
808 10.1080/10256016.2016.1186671, 2017.

809 Kendall, C., and Coplen, T. B.: Distribution of oxygen-18 and deuterium in river waters across
810 the United States, *Hydrological Processes*, 15, 1363-1393, 10.1002/hyp.217, 2001.

811 Klaus, J., and McDonnell, J. J.: Hydrograph separation using stable isotopes: Review and
812 evaluation, *Journal of Hydrology*, 505, 47-64, 10.1016/j.jhydrol.2013.09.006, 2013.

813 Knapp, J. L. A., Neal, C., Schlumpf, A., Neal, M., and Kirchner, J. W.: New water fractions and
814 transit time distributions at Plynlimon, Wales, estimated from stable water isotopes in
815 precipitation and streamflow, *Hydrology and Earth System Sciences*, 23, 4367-4388,
816 10.5194/hess-23-4367-2019, 2019.

817 Kong, Y., Wang, K., Pu, T., and Shi, X.: Nonmonsoon Precipitation Dominates Groundwater
818 Recharge Beneath a Monsoon-Affected Glacier in Tibetan Plateau, *Journal of Geophysical*
819 *Research: Atmospheres*, 124, 10913-10930, 10.1029/2019jd030492, 2019.

820 Laudon, H., Taberman, I., Ågren, A., Futter, M., Ottosson-Löfvenius, M., and Bishop, K.: The
821 Krycklan Catchment Study-A flagship infrastructure for hydrology, biogeochemistry, and
822 climate research in the boreal landscape, *Water Resources Research*, 49, 7154-7158,
823 10.1002/wrcr.20520, 2013.

824 Li, Z.-J., Li, Z.-X., Song, L.-L., Gui, J., Xue, J., Zhang, B. J., and Gao, W. D.: Hydrological
825 and runoff formation processes based on isotope tracing during ablation period in the
826 source regions of Yangtze River, *Hydrology and Earth System Sciences*, 24, 4169-4187,
827 10.5194/hess-24-4169-2020, 2020.

828 Li, Z., Feng, Q., Li, Z., Yuan, R., Gui, J., and Lv, Y.: Climate background, fact and hydrological
829 effect of multiphase water transformation in cold regions of the western china: a review,
830 *EARTH SCIENCE REVIEWS*, 190, 33-57,

831 <https://doi.org/10.1016/j.earscirev.2018.12.004>, 2019.

832 Liu, S.: The second glacier inventory dataset of China (version 1.0) (2006–2011), National
833 Tibetan Plateau Data Center [data set], <https://doi.org/10.3972/glacier.001.2013.db>, 2012.

834 Liu, Z., Tian, L., Yao, T., Gong, T., Yin, C., and Yu, W.: Temporal and spatial variations of delta
835 O-18 in precipitation of the Yarlung Zangbo River Basin, *J. Geogr. Sci.*, 17, 317–326,
836 <https://doi.org/10.1007/s11442-007-0317-1>, 2007.

837 Lutz, A. F., Immerzeel, W. W., Shrestha, A. B., and Bierkens, M. F. P.: Consistent increase in
838 High Asia's runoff due to increasing glacier melt and precipitation, *Nature Climate Change*,
839 4, 587-592, [10.1038/nclimate2237](https://doi.org/10.1038/nclimate2237), 2014.

840 McGuire, K. J., and McDonnell, J. J.: A review and evaluation of catchment transit time
841 modeling, *Journal of Hydrology*, 330, 543-563, [10.1016/j.jhydrol.2006.04.020](https://doi.org/10.1016/j.jhydrol.2006.04.020), 2006.

842 McGuire, K. J., Weiler, M., and McDonnell, J. J.: Integrating tracer experiments with modeling
843 to assess runoff processes and water transit times, *Advances in Water Resources*, 30, 824-
844 837, [10.1016/j.advwatres.2006.07.004](https://doi.org/10.1016/j.advwatres.2006.07.004), 2007.

845 Myneni, R., Knyazikhin, Y., and Park, T.: MOD15A2H MODIS/Terra Leaf Area Index/FPAR
846 8-Day L4 Global 500m SIN Grid V006, NASA EOSDIS Land Processes DAAC [data set],
847 <https://doi.org/10.5067/MODIS/MOD15A2H.006>, 2015.

848 Nan, Y., Tian, F., Hu, H., Wang, L., and Zhao, S.: Stable Isotope Composition of River Waters
849 across the World, *Water*, 11, 1760, [10.3390/w11091760](https://doi.org/10.3390/w11091760), 2019.

850 Nan, Y., He, Z., Tian, F., Wei, Z., and Tian, L.: Can we use precipitation isotope outputs of
851 isotopic general circulation models to improve hydrological modeling in large
852 mountainous catchments on the Tibetan Plateau?, *Hydrology and Earth System Sciences*,
853 25, 6151-6172, [10.5194/hess-25-6151-2021](https://doi.org/10.5194/hess-25-6151-2021), 2021b.

854 Nan, Y., Tian, L., He, Z., Tian, F., and Shao, L.: The value of water isotope data on improving
855 process understanding in a glacierized catchment on the Tibetan Plateau, *Hydrology and*
856 *Earth System Sciences*, 25, 3653-3673, [10.5194/hess-25-3653-2021](https://doi.org/10.5194/hess-25-3653-2021), 2021a.

857 Niinikoski, P. I. A., Hendriksson, N. M., and Karhu, J. A.: Using stable isotopes to resolve
858 transit times and travel routes of river water: a case study from southern Finland, *Isotopes*
859 *in environmental and health studies*, 52, 380-392, [10.1080/10256016.2015.1107553](https://doi.org/10.1080/10256016.2015.1107553), 2016.

860 Ohlanders, N., Rodriguez, M., and McPhee, J.: Stable water isotope variation in a Central
861 Andean watershed dominated by glacier and snowmelt, *Hydrology and Earth System*
862 *Sciences*, 17, 1035-1050, [10.5194/hess-17-1035-2013](https://doi.org/10.5194/hess-17-1035-2013), 2013.

863 Pomeroy, J. W., Gray, D. M., Brown, T., Hedstrom, N. R., Quinton, W. L., Granger, R. J., and
864 Carey, S. K.: The cold regions hydrological model: a platform for basing process
865 representation and model structure on physical evidence, *Hydrological Processes*, 21,
866 2650-2667, [10.1002/hyp.6787](https://doi.org/10.1002/hyp.6787), 2007.

867 Rai, S. P., Singh, D., Jacob, N., Rawat, Y. S., Arora, M., and BhishmKumar: Identifying

868 contribution of snowmelt and glacier melt to the Bhagirathi River (Upper Ganga) near
869 snout of the Gangotri Glacier using environmental isotopes, *Catena*, 173, 339-351,
870 10.1016/j.catena.2018.10.031, 2019.

871 Reggiani, P., Hassanizadeh, S. M., Sivapalan, M., and Gray, W. G.: A unifying framework for
872 watershed thermodynamics: constitutive relationships, *Advances In Water Resources*, 23,
873 15-39, 10.1016/s0309-1708(99)00005-6, 1999.

874 Son, K., and Sivapalan, M.: Improving model structure and reducing parameter uncertainty in
875 conceptual water balance models through the use of auxiliary data, *Water Resources*
876 *Research*, 43, 10.1029/2006wr005032, 2007.

877 Sprenger, M., Stumpp, C., Weiler, M., Aeschbach, W., Allen, S. T., Benettin, P., Dubbert, M.,
878 Hartmann, A., Hrachowitz, M., Kirchner, J. W., McDonnell, J. J., Orłowski, N., Penna, D.,
879 Pfahl, S., Rinderer, M., Rodriguez, N., Schmidt, M., and Werner, C.: The Demographics
880 of Water: A Review of Water Ages in the Critical Zone, *Reviews Of Geophysics*, 57, 800-
881 834, 10.1029/2018rg000633, 2019.

882 Stevenson, J. L., Birkel, C., Neill, A. J., Tetzlaff, D., and Soulsby, C.: Effects of streamflow
883 isotope sampling strategies on the calibration of a tracer-aided rainfall-runoff model,
884 *Hydrological Processes*, 35, 10.1002/hyp.14223, 2021.

885 Tan, H., Chen, X., Shi, D., Rao, W., Liu, J., Liu, J., Eastoe, C. J., and Wang, J.: Base flow in the
886 Yarlungzangbo River, Tibet, maintained by the isotopically-depleted precipitation and
887 groundwater discharge, *The Science of the total environment*, 759, 143510,
888 10.1016/j.scitotenv.2020.143510, 2021.

889 Tetzlaff, D., Birkel, C., Dick, J., Geris, J., and Soulsby, C.: Storage dynamics in
890 hydrogeological units control hillslope connectivity, runoff generation, and the evolution
891 of catchment transit time distributions, *Water Resour Res*, 50, 969-985,
892 10.1002/2013WR014147, 2014.

893 Tian, F., Hu, H., Lei, Z., and Sivapalan, M.: Extension of the Representative Elementary
894 Watershed approach for cold regions via explicit treatment of energy related processes,
895 *Hydrology And Earth System Sciences*, 10, 619-644, 10.5194/hess-10-619-2006, 2006.

896 Tian, F., Xu, R., Nan, Y., Li, K., and He, Z.: Quantification of runoff components in the Yarlung
897 Tsangpo River using a distributed hydrological model, *Advances in Water Science*, 31,
898 324-336, 2020.

899 Tong, R., Parajka, J., Salentinig, A., Pfeil, I., Komma, J., Széles, B., Kubáň, M., Valent, P.,
900 Vreugdenhil, M., Wagner, W., and Blöschl, G.: The value of ASCAT soil moisture and
901 MODIS snow cover data for calibrating a conceptual hydrologic model, *Hydrology and*
902 *Earth System Sciences*, 25, 1389-1410, 10.5194/hess-25-1389-2021, 2021.

903 Viviroli, D., Weingartner, R., and Messerli, B.: Assessing the hydrological significance of the
904 world's mountains, *Mountain Research And Development*, 23, 32-40, 10.1659/0276-

905 4741(2003)023[0032:athsot]2.0.co;2, 2003.

906 Wang, C., Dong, Z., Qin, X., Zhang, J., Du, W., and Wu, J.: Glacier meltwater runoff process
907 analysis using δD and $\delta^{18}O$ isotope and chemistry at the remote Laohugou glacier basin
908 in western Qilian Mountains, China, *Journal of Geographical Sciences*, 26, 722-734,
909 10.1007/s11442-016-1295-y, 2016.

910 Wang, Y., Wang, L., Zhou, J., Yao, T., Yang, W., Zhong, X., Liu, R., Hu, Z., Luo, L., Ye, Q.,
911 Chen, N., and Ding, H.: Vanishing Glaciers at Southeast Tibetan Plateau Have Not Offset
912 the Declining Runoff at Yarlung Zangbo, *Geophysical Research Letters*, 48,
913 10.1029/2021gl094651, 2021.

914 Wolfe, B. B., Karst-Riddoch, T. L., Hall, R. I., Edwards, T. W. D., English, M. C., Palmini, R.,
915 McGowan, S., Leavitt, P. R., and Vardy, S. R.: Classification of hydrological regimes of
916 northern floodplain basins (Peace–Athabasca Delta, Canada) from analysis of stable
917 isotopes ($\delta^{18}O$, δ^2H) and water chemistry, *Hydrological Processes*, 21, 151-168,
918 10.1002/hyp.6229, 2007.

919 Xi, X.: A Review of Water Isotopes in Atmospheric General Circulation Models: Recent
920 Advances and Future Prospects, *International Journal of Atmospheric Sciences*, 2014, 1-
921 16, 10.1155/2014/250920, 2014.

922 Xia, X., Li, S., Wang, F., Zhang, S., Fang, Y., Li, J., Michalski, G., and Zhang, L.: Triple oxygen
923 isotopic evidence for atmospheric nitrate and its application in source identification for
924 river systems in the Qinghai-Tibetan Plateau, *The Science of the total environment*, 688,
925 270-280, 10.1016/j.scitotenv.2019.06.204, 2019.

926 Xu, R., Hu, H., Tian, F., Li, C., and Khan, M. Y. A.: Projected climate change impacts on future
927 streamflow of the Yarlung Tsangpo-Brahmaputra River, *Global and Planetary Change*, 175,
928 144-159, 10.1016/j.gloplacha.2019.01.012, 2019.

929 Yang, K. and He, J.: China meteorological forcing dataset (1979–2018), National Tibetan
930 Plateau Data Center [data set],
931 <https://doi.org/10.11888/AtmosphericPhysics.tpe.249369.file>, 2019.

932 Yao, T., Masson-Delmotte, V., Gao, J., Yu, W., Yang, X., Risi, C., Sturm, C., Werner, M., Zhao,
933 H., He, Y., Ren, W., Tian, L., Shi, C., and Hou, S.: A review of climatic controls on $\delta^{18}O$
934 in precipitation over the Tibetan Plateau: Observations and simulations, *Reviews of
935 Geophysics*, 51, 525-548, 10.1002/rog.20023, 2013.

936 Yde, J. C., Knudsen, N. T., Steffensen, J. P., Carrivick, J. L., Hasholt, B., Ingeman-Nielsen, T.,
937 Kronborg, C., Larsen, N. K., Mernild, S. H., Oerter, H., Roberts, D. H., and Russell, A. J.:
938 Stable oxygen isotope variability in two contrasting glacier river catchments in Greenland,
939 *Hydrology and Earth System Sciences*, 20, 1197-1210, 10.5194/hess-20-1197-2016, 2016.

940 Yong, B., Wang, C.-Y., Chen, J., Chen, J., Barry, D. A., Wang, T., and Li, L.: Missing water
941 from the Qiangtang Basin on the Tibetan Plateau, *Geology*, 49, 867-872, 10.1130/g48561.1,

942 2021.

943 Yoshimura, K., Kanamitsu, M., Noone, D., and Oki, T.: Historical isotope simulation using
944 Reanalysis atmospheric data, *Journal of Geophysical Research*, 113,
945 10.1029/2008jd010074, 2008.

946 Zhang, F., Zhang, H. B., Hagen, S. C., Ye, M., Wang, D. B., Gui, D. W., Zeng, C., Tian, L. D.,
947 and Liu, J. S.: Snow cover and runoff modelling in a high mountain catchment with scarce
948 data: effects of temperature and precipitation parameters, *Hydrol. Process.*, 29, 52–65,
949 <https://doi.org/10.1002/hyp.10125>, 2015.

950 Zhang, Z., Chen, X., Cheng, Q., and Soulsby, C.: Storage dynamics, hydrological connectivity
951 and flux ages in a karst catchment: conceptual modelling using stable isotopes, *Hydrology
952 and Earth System Sciences*, 23, 51-71, 10.5194/hess-23-51-2019, 2019.

953

954 **List of Tables**

955

956 **Table 1.** Summary of precipitation and stream water samples in the YTR and KR catchments.

Catchment (Station)	Year	Sampling period	Precipitation			Stream		
			Sample number	$\overline{\delta^{18}\text{O}}$ (‰)	Std (‰)	Sample number	$\overline{\delta^{18}\text{O}}$ (‰)	Std (‰)
YTR (Nuxia)	2005	14/Mar to 23/Oct	86	-10.33	7.18	34	-15.74	1.60
YTR (Yangcun)		17/Mar to 05/ Oct	59	-13.17	7.10	30	-16.57	1.69
YTR (Nugesha)		14/Mar to 22/ Oct	45	-14.29	7.99	25	-17.84	0.99
YTR (Lazi)		06/ Jun to 22/Sep	42	-17.41	5.75	22	-16.52	1.43
	2006	06/Apr to 11/Nov	24	-15.22	3.83	31	-17.35	1.68
	2007	23/Apr to 09/ Oct	39	-16.99	5.93	25	-17.30	1.01
KR (Wengguo)	2010	05/May to 18/ Oct	63	-19.25	5.03	23	-17.44	1.29
	2011	28/Mar to 06/Nov	69	-13.99	5.90	32	-17.11	1.30
	2012	16/ Jun to 22/ Sep	42	-13.88	6.21	14	-17.01	0.60

957

959 **Table 2.** Calibrated parameters of the THREW-T model

Symbol	Unit	Physical descriptions	Value range
nt	-	Manning roughness coefficient for hillslope	0-0.2
WM	cm	Tension water storage capacity, used in Xinanjiang model to calculate saturation area	0-10
B	-	Shape coefficient used in Xinanjiang model to calculate saturation area	0-1
KKA	-	Coefficient to calculate subsurface runoff in $Rg=KKD \cdot S \cdot K^S_s \cdot (y_s/Z)^{KKA}$, where S is the topographic slope, K^S_s is the saturated hydraulic conductivity, y_s is the depth of saturated groundwater, Z is the total soil depth	0-6
KKD	-	See description for KKA	0-0.5
T_0	°C	Temperature threshold above which snow and glacier melt	-5-5
DDF_N	mm/°C/day	Degree day factor for snowmelt	0-10
DDF_G	mm/°C/day	Degree day factor for glacier melt	0-10
$C1$	-	Coefficient to calculate the runoff concentration process using Muskingum method: $O_2=C_1 \cdot I_1+C_2 \cdot I_2+C_3 \cdot O_1+C_4 \cdot Q_{lat}$, where I_1 and O_1 is the inflow and outflow at prior step, I_2 and O_2 is the inflow and outflow at current step, Q_{lat} is lateral flow of the river channel, $C_3=I-C_1-C_2$, $C_4=C_1+C_2$	0-1
$C2$	-	See description for $C1$	0-1

Table 3. Descriptions of water sampling scenarios in the three numerical experiments. $\delta^{18}\text{O}_{\text{GM}}$ is the assumed glacier meltwater isotope signature and $\overline{\delta^{18}\text{O}_{\text{PR}}}$ refers to the long term mean isotope signature of precipitation.

Experiment	Scenarios	Isotope data conditions
Benchmark model running in the YTR basin	BM_YTR	Using assumed glacier meltwater isotope as: $\delta^{18}\text{O}_{\text{GM}} = \overline{\delta^{18}\text{O}_{\text{PR}}} - 5\%$ Using IsoGSM outputs that were merged with sample measurements of precipitation isotope from four sampling sites Using all available stream water samples in the study period to calibrate the model
Benchmark model running in the KR catchment	BM_KR	Using all available stream water samples in the study period to calibrate the model
Experiment 1: Estimate of glacier meltwater isotope	G_Δ1	Assuming glacier meltwater isotope as: $\delta^{18}\text{O}_{\text{GM}} = \overline{\delta^{18}\text{O}_{\text{PR}}} - 1\%$
	G_Δ3	Assuming glacier meltwater isotope as: $\delta^{18}\text{O}_{\text{GM}} = \overline{\delta^{18}\text{O}_{\text{PR}}} - 3\%$
	G_Δ7	Assuming glacier meltwater isotope as: $\delta^{18}\text{O}_{\text{GM}} = \overline{\delta^{18}\text{O}_{\text{PR}}} - 7\%$
	G_Δ9	Assuming glacier meltwater isotope as: $\delta^{18}\text{O}_{\text{GM}} = \overline{\delta^{18}\text{O}_{\text{PR}}} - 9\%$
Experiment 2: Site sampling data of precipitation isotope	P_1station	Using IsoGSM outputs merged with measurements of precipitation isotope collected at one station (Nuxia) in YTR
	P_2stationNY	Using IsoGSM outputs merged with measurements of precipitation isotope collected at two stations (Nuxia and Yangcun) in YTR
	P_2stationNL	Using IsoGSM outputs merged with measurements of precipitation isotope collected at two stations (Nuxia and Lazi) in YTR
Experiment 3: Stream water sampling strategy for model evaluation	RT_YTR_BM	Sampling strategy: time series sampling; Sampling timing: wet season; Sampling frequency: weekly; Duration of sampling period: 1 year (2005); Number of sampling site: 1 station (Nuxia)
	RT_YTR_WholeYear	Same to RT_YTR_BM, but with the sampling timing as the whole study years
	RT_YTR_Monthly	Same to RT_YTR_BM, but with the sampling frequency as monthly
	RT_YTR_2year	Same to RT_YTR_BM, but with the duration of sampling period as only 2 years (2005 and 2006)
	RT_YTR_3year	Same to RT_YTR_BM, but with the duration of sampling period as only 3 years (2005-2007)
	RT_YTR_2station	Same to RT_YTR_BM, but with the number of sampling site as 2 stations (Nuxia and Yangcun)
	RT_YTR_4station	Same to RT_YTR_BM, but with the number of sampling site as 4 stations (Nuxia, Yangcun, Nugesha and Lazi)
	RS_YTR_Main	Sampling strategy: spatially distributed sampling in a single field campaign; Location of sampling site: along the main stream
	RS_YTR_Tributary	Same to RS_YTR_Main, but using stream water samples from additional sites along the tributaries
	RT_KR_1year	Sampling strategy: time series sampling; Duration of sampling period: 1 year (2006)
	RT_KR_2year	Same to RT_KR_1year, but with the duration of sampling period as 2 years (2006 and 2007)
	RT_KR_3year	Same to RT_KR_1year, but with the duration of sampling period as 3 years (2006-2007, 2010)
	RT_KR_4year	Same to RT_KR_1year, but with the duration of sampling period as 4 years (2006-2007, 2010-2011)
RT_KR_5year	Same to RT_KR_1year, but with the duration of sampling period as 5 years (2006-2007, 2010-2012)	

964 **Table 4.** Contributions (%) of runoff components in the YTR basin and KR catchment
 965 estimated by different calibration variants in the benchmark scenario.

Runoff Component	YTR basin		KR catchment	
	Bi-objective calibration*	Tri-objective calibration	Bi-objective calibration	Tri-objective calibration
Rainfall	62.8 (± 6.5)	70.7 (± 2.5)	46.4 (± 5.0)	43.9 (± 1.4)
Snowmelt	10.8 (± 1.1)	12.2 (± 0.4)	22.6 (± 2.4)	21.4 (± 0.7)
Glacier melt	26.4 (± 7.5)	17.1 (± 2.9)	31.0 (± 7.4)	34.6 (± 2.0)
Surface runoff	52.1 (± 10.5)	44.7 (± 6.7)	62.0 (± 10.9)	75.1 (± 3.3)
Subsurface runoff	47.9 (± 10.5)	55.3 (± 6.7)	38.0 (± 10.5)	24.9 (± 3.3)

966 *: Values in brackets refer to the standard deviation of the contribution of runoff component produced
 967 by the behavioral parameter sets.

968

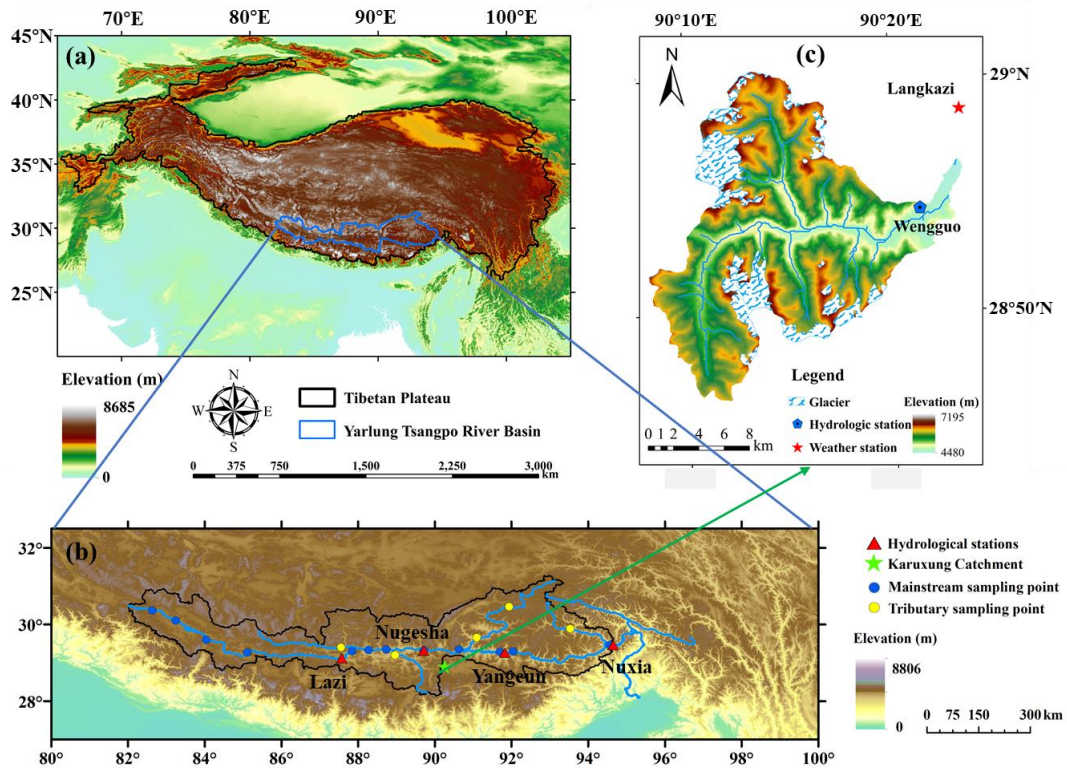
969 **Table 5.** Benchmark parameter set and corresponding model behavior that are used to produce
 970 stream water $\delta^{18}\text{O}$ data for model calibration in experiment 3 in YTR basin.

Parameter value		Model behavior	
<i>nt</i>	0.09	NSE _{dis} (Nuxia,calibration)	0.87
<i>WM</i>	0.92	NSE _{dis} (Nuxia,validation)	0.80
<i>B</i>	0.62	RMSE _{SCA} (calibration)	0.08
<i>KKa</i>	3.22	RMSE _{SCA} (validation)	0.12
<i>KKD</i>	0.14	NSE _{iso}	0.58
<i>T₀</i>	1.59	NSE _{dis} (Yangcun)	0.85
<i>DDF_N</i>	8.04	NSE _{dis} (Nugesha)	0.76
<i>DDF_G</i>	8.28	Contribution of rainfall	70%
<i>C1</i>	0.0004	Contribution of snowmelt	12%
<i>C2</i>	0.075	Contribution of glacier melt	18%
		Contribution of baseflow	56%

971

972 List of Figures

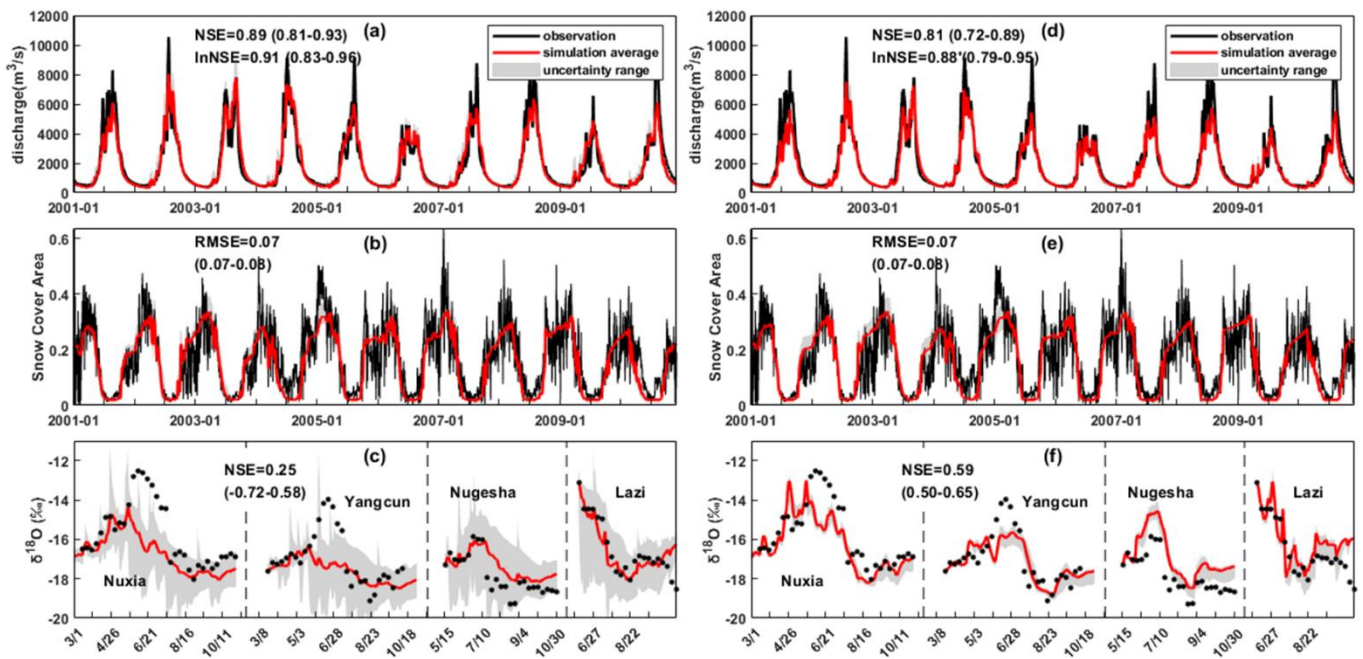
973



974

975 **Figure 1.** Locations and topography of the (a) Tibetan Plateau, (b) Yarlung Tsangpo river
976 basin and (c) Karuxung catchment. Triangles in figure b refer to hydrometric stations and
977 sampling sites for precipitation and stream water isotope. Dots in figure b refer to assumed
978 stream water sampling locations in RD_YTR scenarios.

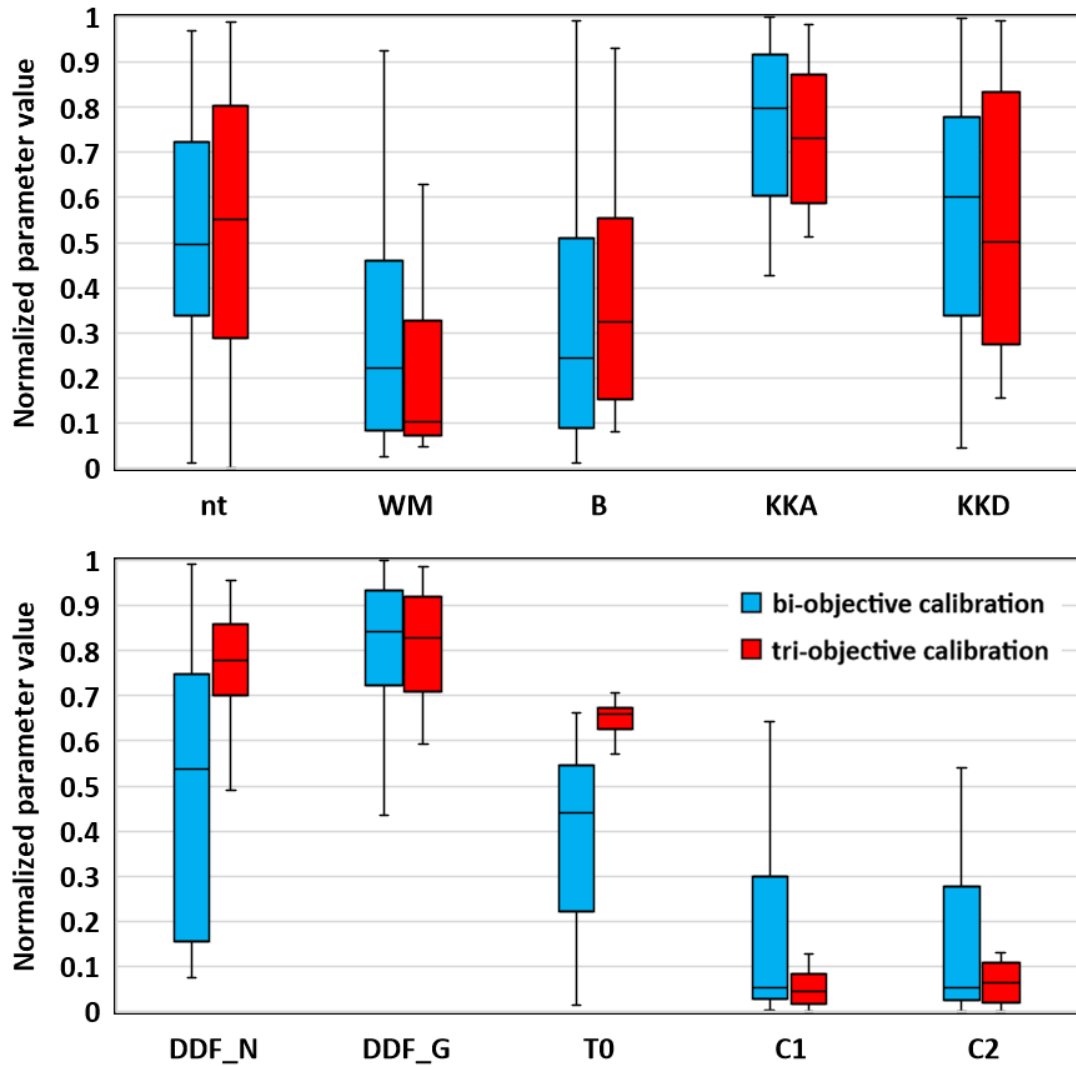
979



980

981 **Figure 2.** Uncertainty ranges and metrics values of the simulated discharge (Nuxia station),
 982 SCA, and stream $\delta^{18}\text{O}$ (at four stations during 2005) in the YTR basin, that were produced by
 983 the behavioral parameter sets of a bi-objective calibration (a-c) and a tri-objective (d-f)
 984 calibration in the benchmark model running.

985



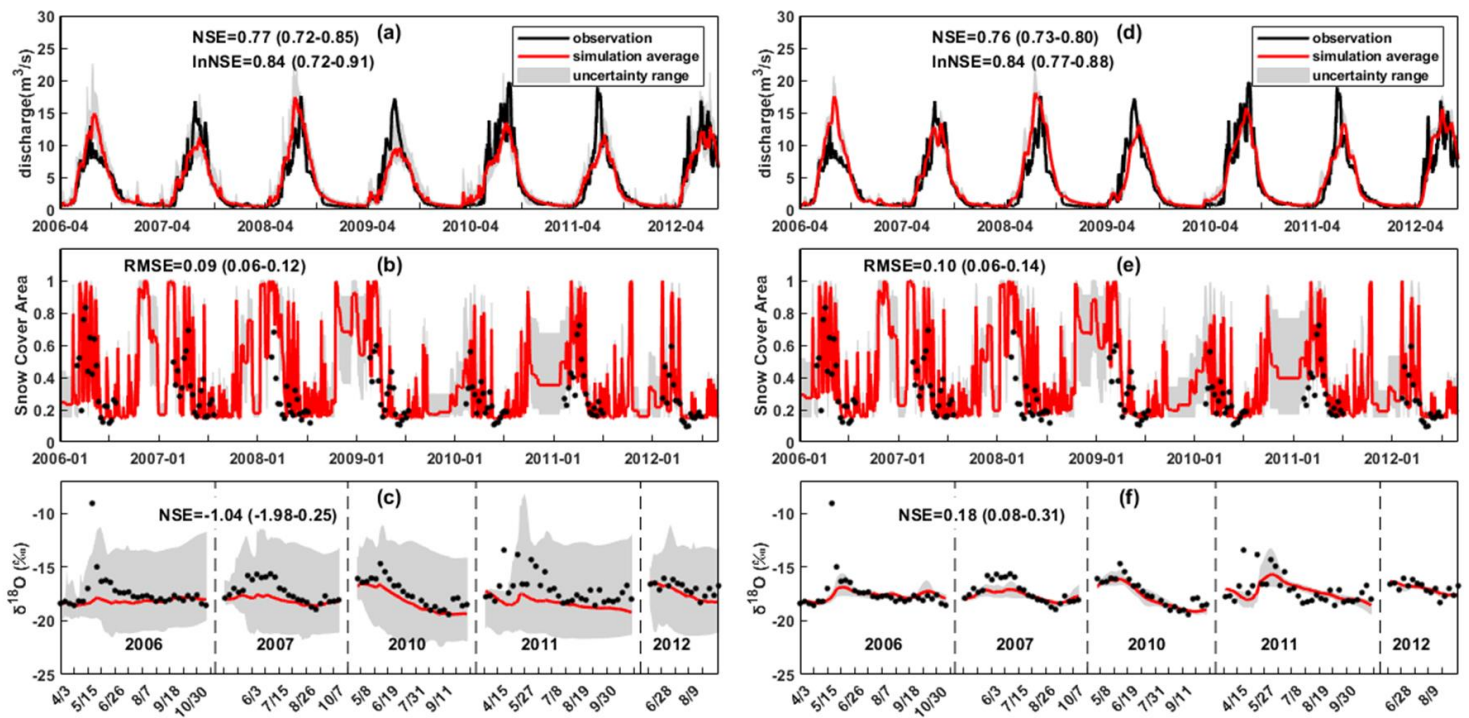
986

987

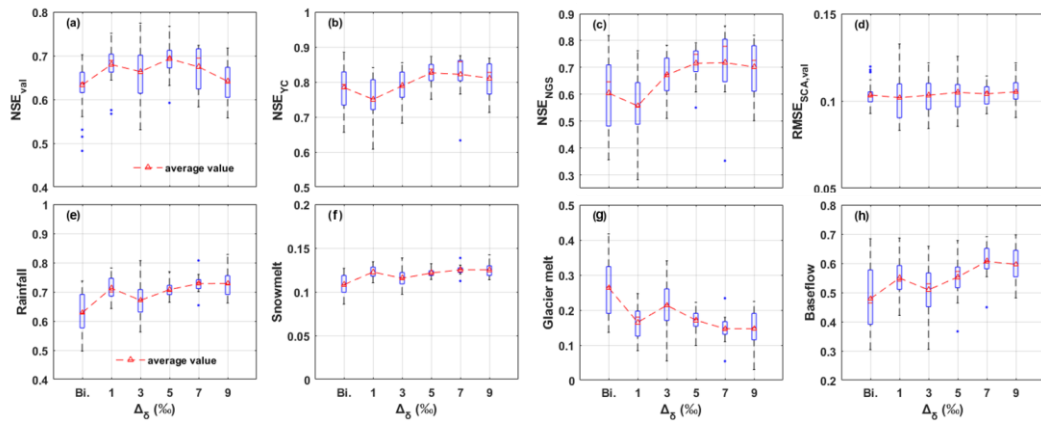
Figure 3. Uncertainties of behavioral parameter set obtained by bi- and tri-objective calibration methods for BM_YTR scenario in YTR basin.

988

989



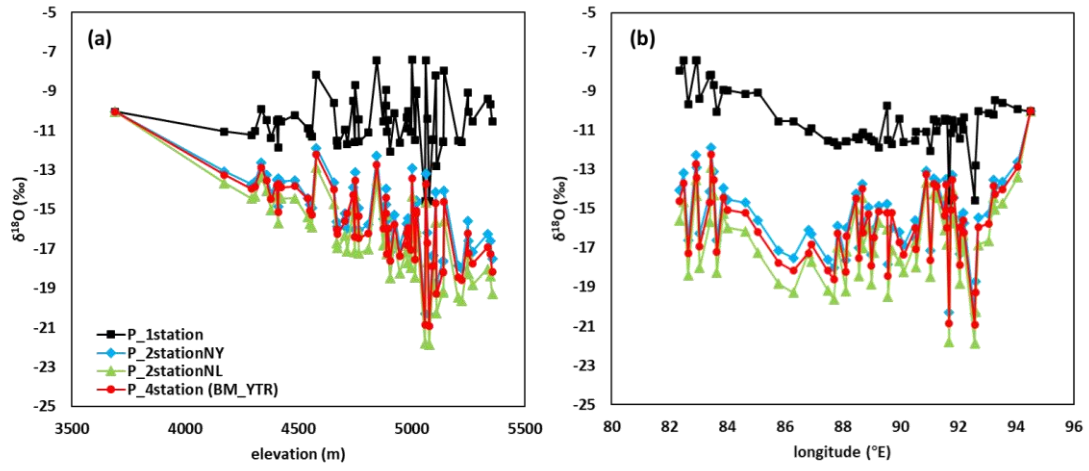
990 **Figure 4.** Uncertainty ranges and metrics values of the simulated discharge, SCA, and stream
 991 $\delta^{18}\text{O}$ in the KR catchment produced by the behavioral parameter sets of a bi-objective
 992 calibration (a-c) and a tri-objective (d-f) calibration in the benchmark model running.



994

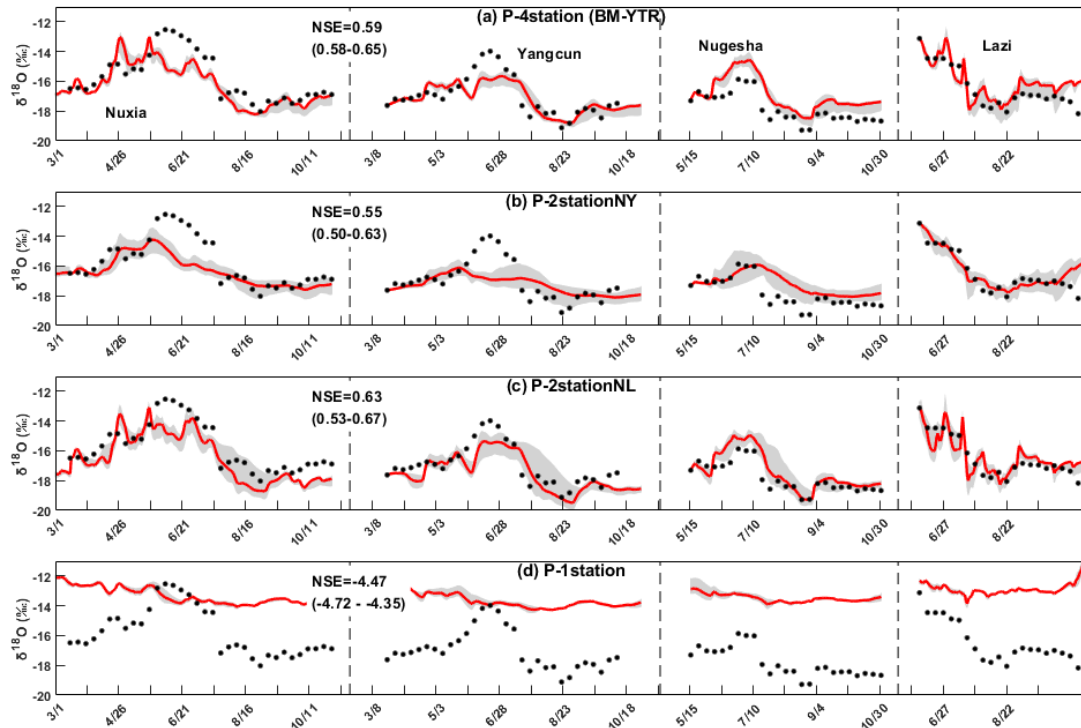
995 **Figure 5.** Model performances (a-d) and runoff component contributions (e-h) in the YTR basin
 996 in different scenarios using different glacier isotope input (experiment 1). Subplot (a) and (d)
 997 are the performances for Nuxia streamflow and SCA simulation in validation period,
 998 respectively. Subplot (b) and (c) are the performances for streamflow simulation at internal
 999 stations Yangcun and Nugesha, respectively. Subplot (e), (f) and (g) are the contribution of
 1000 runoff components based on water source definition. Subplot (h) is the contribution of baseflow
 1001 based on the runoff pathway definition.

1002



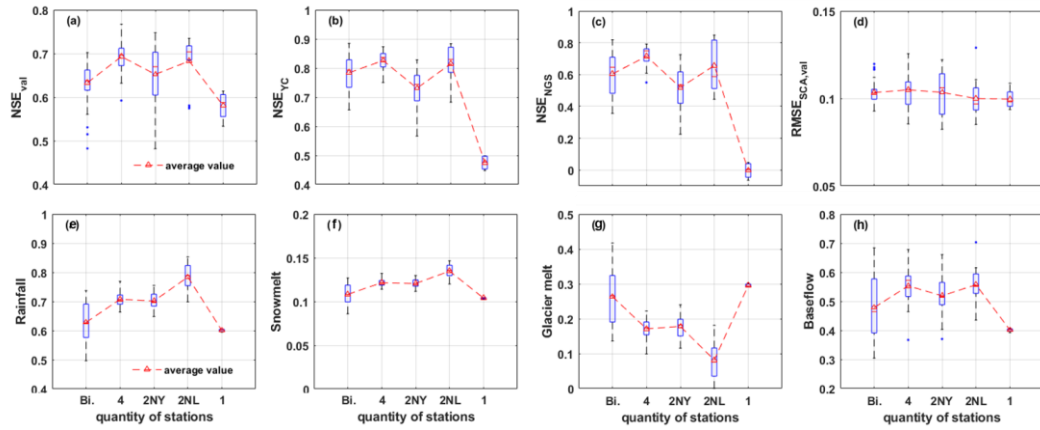
1003
 1004
 1005
 1006

Figure 6. Comparisons of weighted averages of precipitation $\delta^{18}\text{O}$ on 63 REWs in the YTR by elevation (a) and longitude (b) in each scenario of experiment 2.



1007
 1008
 1009
 1010

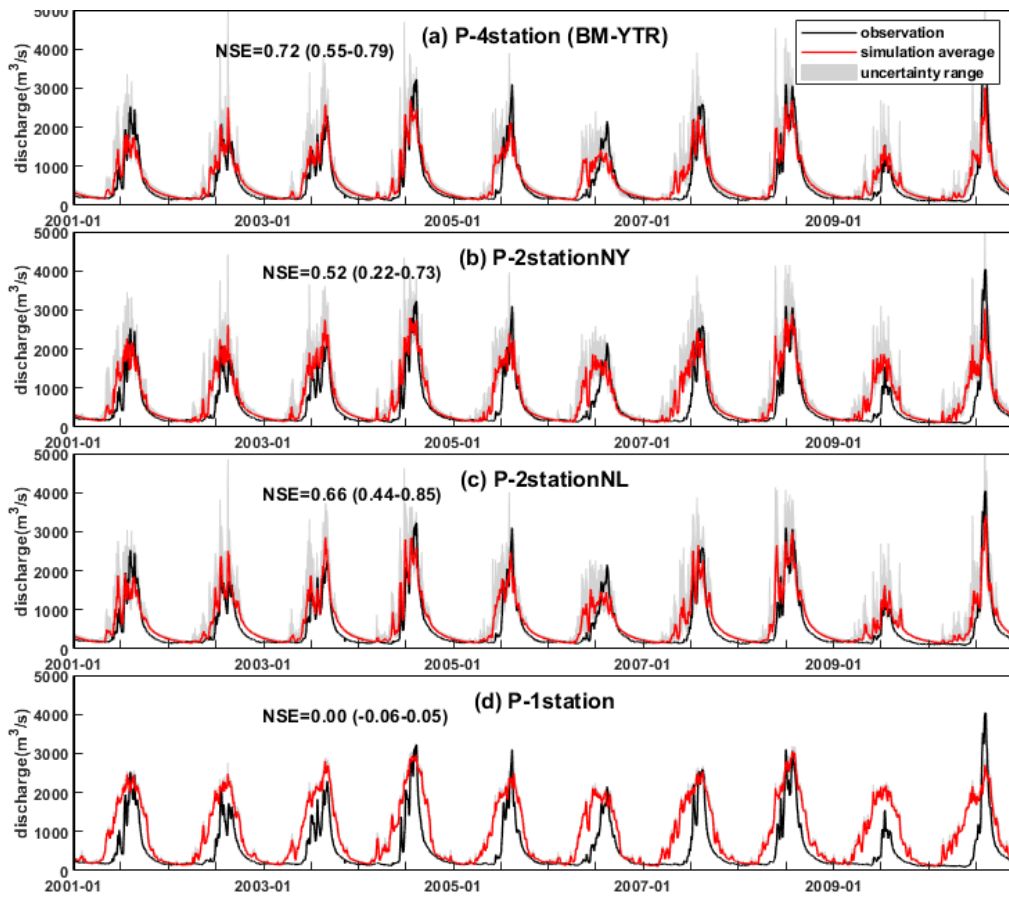
Figure 7. Uncertainty ranges of stream water $\delta^{18}\text{O}$ simulations at four stations in 2005 produced by the behavioral parameter sets of each scenario in experiment 2.



1011
 1012
 1013
 1014
 1015
 1016
 1017
 1018
 1019

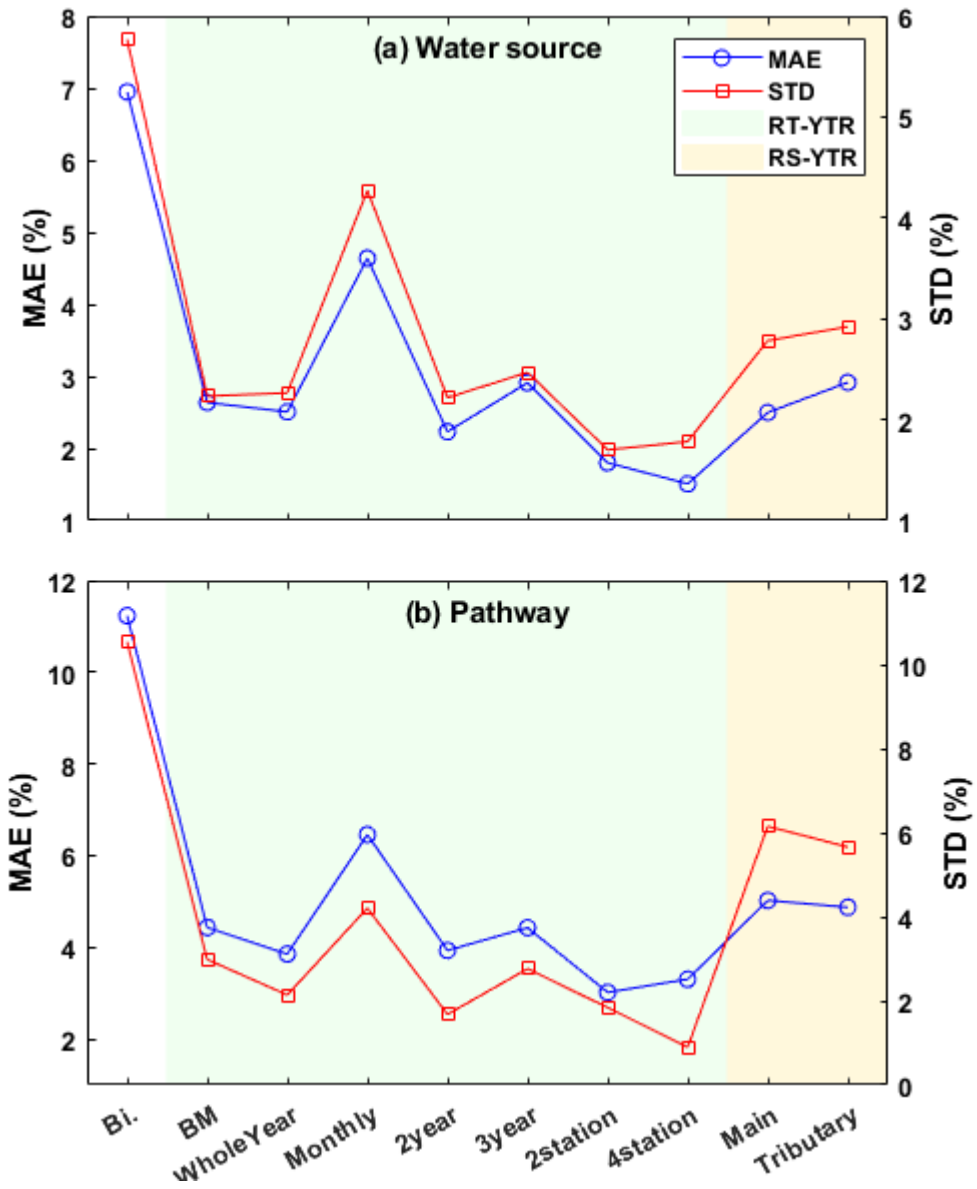
Figure 8. Model performances (a-d) and runoff component contributions (e-h) in the YTR basin in different scenarios using precipitation isotope measurements from different sampling sites (experiment 2). Subplot (a) and (d) are the performances for Nuxia streamflow and SCA simulation in validation period, respectively. Subplot (b) and (c) are the performances for streamflow simulation at internal stations Yangcun and Nugesha, respectively. Subplot (e), (f) and (g) are the contribution of runoff components based on water source definition. Subplot (h) is the contribution of baseflow based on the runoff pathway definition.

1020



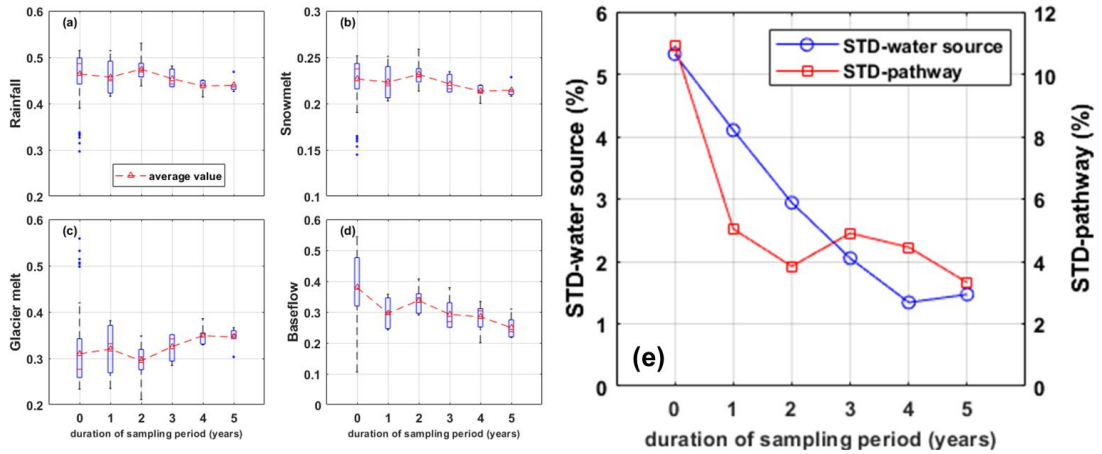
1021

1022 **Figure 9.** Uncertainty range and metrics values of simulated discharge at Nugesha station
1023 produced by the behavioral parameter sets of each scenario in experiment 2.
1024



1025
 1026
 1027
 1028
 1029
 1030

Figure 10. Accuracy and uncertainty metrics of estimated CRCs in the YTR basin derived from the different stream water sampling strategies (experiment 3). (a) for CRCs quantified under the definition of water source and (b) for CRCs quantified under the definition of runoff pathway.



1031

1032 **Figure 11.** Uncertainties of the contributions of (a) rainfall, (b) snowmelt, (c) glacier melt and
 1033 (d) baseflow in the KR catchment, estimated by scenarios with different durations of sampling
 1034 period (experiment 3). The uncertainties of CRCs based on two different definitions are
 1035 summarized in subplot (e).

1036